Tropical lows in southern Africa: tracks, rainfall contributions and the role of ENSO

Article

Published Version

It is advisable to refer to the publisher's version if you intend to cite from the work. See Guidance on citing.

To link to this article DOI: http://dx.doi.org/10.1029/2019JD030803

Publisher: American Geophysical Union

www.reading.ac.uk/centaur

CentAUR

Correspondence to:
E. Howard,
emma.howard@ouce.ox.ac.uk

Tropical Lows in Southern Africa: Tracks, Rainfall Contributions, and the Role of ENSO

Emma Howard[1] , Richard Washington[1] , and Kevin I. Hodges[2]

[1]School of Geography and the Environment, University of Oxford, Oxford, UK, [2]Department of Meteorology, University of Reading, Reading, UK

Abstract Southern African tropical lows are synoptic-scale cyclonic vortices that propagate westward across southern Africa in the Austral summer. They strongly influence local rainfall and aggregate in the climatological December, January, and February mean to form the Angola Low. In this study, tropical lows are identified and tracked using an objective feature tracking method. The statistics of tropical low tracks over southern Africa are presented and compared across three reanalysis products. Findings are compared to the literature of tropical low-pressure areas elsewhere in the world, where it is found that most tracking statistics compare well but that the tendency of tropical lows to become semistationary over Angola is unique to southern Africa. The hypothesis that tropical lows in Angola have a causal relationship with Tropical Temperate Troughs is tested, and a correlation between occurrence frequencies is found at interannual but not daily time scales. Precipitation is attributed to the tropical lows, and it is found that tropical lows are associated with 31% of rainfall across tropical southern Africa, based on gridded precipitation products. The interannual variability of the number of tropical lows that form per year ($\sigma = 6$ events/year) is linked to El Niño–Southern Oscillation (ENSO) and the tropical easterly jet. The mean latitude of tropical lows is shifted northward during El Niño and southward during La Niña. Much of the interannual precipitation variability maximum in Angola is attributed to rainfall associated with tropical lows. These results provide insights into the southern African response to ENSO and into the mechanisms of rainfall in the southern African tropical edge.

Plain Language Summary Tropical lows are storms that are a bit like very weak tropical cyclones. They occur in summer in tropical regions. This paper tracks individual tropical lows across southern Africa in weather records from the last 39 years. We then look at how they behave, how much they rain, whether they interact with other storms, and how they vary from year to year. About 33 tropical lows are found each year, and they tend to cluster in eastern Angola. We find that 31% of rainfall in the region surrounding Angola and Zambia comes from tropical lows. The number of tropical lows that form in a summer is really important for whether that summer will be unusually dry or wet, particularly along the northern border of Namibia. The number of tropical lows that form in each year is related to the El Niño–Southern Oscillation and also to the winds high up in the atmosphere. In the El Niño phase of El Niño–Southern Oscillation cycle, which usually causes drought in southern Africa, tropical lows form less frequently and further north. In the La Niña phase, which is usually wet in southern Africa, tropical lows form more frequently and further south.

1. Introduction

The southern "tropical edge" of the African rain band (16–22° S) is a hot spot of rainfall variability. The tropical edge spans eight countries, and its precipitation feeds the Okavango Delta and the Zambezi river basin. The former is a hot spot of biodiversity (Ramberg et al., 2006), while the latter supports an economy of 30 million people and has been extensively dammed for hydroelectric plants (World Bank, 2010). Quantification of the behavior and rainfall contributions of the local synoptic processes provides important context for understanding interannual variability and future change of regional precipitation.

Tropical lows, middle level cyclonic vortices that form in the tropical easterlies, are one such process that contributes rainfall in the tropical edge. For the purposes of this study, we define the tropical edge as spanning 12–22°S, from the west to the east coast of southern Africa. Tropical lows are well studied across the world, including in India (Godbole, 1977; Hunt et al., 2016; Hurley & Boos, 2015), northern Australiaj

(Kilroy et al., 2017; McBride & Keenan, 1982), and the low-latitude oceans (Fine et al., 2016; Wallace, 1971). When conditions are favorable, tropical lows located over oceans may intensify into tropical cyclones, and so much of the research into tropical lows in general has focused in regions where this occurs, motivated by increasing the predictability of extreme weather risk (e.g., Smith & Montgomery, 2015). However, while tropical lows that exist over land and do not intensify are much less catastrophic than tropical cyclones, they are also more frequent, and so their primary importance to the regional population shifts from being a class of extreme weather events to a source of precipitation (Hunt & Fletcher, 2019; Lavender & Abbs, 2013).

The track statistics of these weather systems and their local contributions to rainfall have been studied across the tropics. In the South Asian monsoon, monsoon depressions are an important source of rainfall in north and west India (Hunt et al., 2016). Typically, two to five systems form each summer and tend to track westward along the southern edge of the Himalayas (Hunt et al., 2016). African easterly waves (AEWs), which form in north Africa, have also been intensely studied (Burpee, 1974; Gomes et al., 2019; Hopsch et al., 2007; Hsieh & Cook, 2005; Thorncroft & Hoskins, 1995) but are significantly larger and more frequent than southern African tropical lows. In northern Australia, closed low-pressure systems contribute up to 60% of precipitation in the Pilbara, and the proportion of precipitation that is attributable to tropical lows increased between 1989 and 2009 (Lavender & Abbs, 2013). Berry et al. (2012) identified monsoon weather systems in northern Australia using the 315-K isotherm of isentropic potential vorticity and found that these systems track westward at 6 m/s and form every 2.5 days in the wet season. Hurley and Boos (2015) conducted a global study of land-based depressions in the tropics and found similar results over northern Australia and India. Howard and Washington (2018) found that the radii and vertical structures of Australian and Indian monsoon lows were qualitatively comparable to those of tropical lows in southern Africa.

The prominence of tropical lows over southern Africa was first described by Taljaard (1953), who noted that these lows are quasi-stationary in the Angola region and are associated with low-level convergence. In the seasonal and climatological means, these systems, along with dry and shallow heat lows, aggregate to create a local pressure minimum which is called the Angola Low (Howard & Washington, 2018; Munday & Washington, 2017). In recent years, the Angola Low has become well known due to statistical correlations to rainfall variability and to Tropical Temperate Trough (TTT) formation on the interannual time scale. Reason et al. (2006) first suggested that the Angola Low modulates the relationship between the El Niño–Southern Oscillation (ENSO) and southern African precipitation. ENSO is the main driver of precipitation variability in southern Africa, with the El Niño phase commonly associated with drought. The contrast between the very strong El Niño of 1998, when the Angola Low was strong and the forecasted drought did not occur, and 2015, when the Angola Low was unusually weak and the summer rainfall was the lowest in recorded history, demonstrates this relationship (Blamey et al., 2018). Howard and Washington (2018) found that it is the contribution of tropical lows to the Angola Low and not that of heat lows, which influences the relationship between rainfall and ENSO.

TTTs are elongated cloud bands that form over southern Africa and provide a large proportion of the subtropical summer rainfall to the south of the tropical edge, where annual rainfall is typically low (Harrison, 1984). TTTs occur when an upper level ridge in the subtropical jet interacts with moist tropical convection from tropical southern Africa and allows convection to spread in a band across the continent (Macron et al., 2014). Since the tropical convection that TTTs are associated with is often in the Angola Low region, it has been hypothesized that the convection that is collected may need to be associated with an Angola tropical low (Todd & Washington, 1999). For example, Hart et al. (2010) identify the importance of tropical lows in three case studies, while Macron et al. (2014) highlight an increase in moisture flux around the Angola Low in lagged TTT composites. However, this relationship has not been studied on a synoptic time scale. Crétat et al. (2018) call for a better understanding of the relationship between the Angola Low and tropical-extratropical interactions on a daily time scale.

Despite being studied based on meteorological analyses before the satellite era (Taljaard, 1972), little work has been done since the availability of reanalysis data sets on systematically characterizing the behavior of tropical lows in southern Africa. While tropical lows are precipitating systems, there have been no attempts to determine the proportion of precipitation that may be attributed to tropical lows or their role in interannual rainfall variability, as compared to other systems such as localized convection, thunderstorms, and mesoscale convective systems. In the intervening years, various tools have been developed to identify and follow atmospheric features in reanalysis data sets as they evolve and move through space. One such tool is

Table 1
Reanalysis and Gridded Rainfall Products

Name	Type	Spatial resolution	Temporal resolution	Temporal coverage	Citation
ERA-5	Reanalysis	T639 (∼0.28° × 0.28°)	Hourly	1979–2018	C3S (2017)
MERRA2	Reanalysis	1.0° × 1.5°	3-hourly	1980–2018	Gelaro et al. (2017)
ERA-Interim	Reanalysis	T255 (∼0.70° × 0.70°)	6-hourly	1979–2018	Dee et al. (2011)
CHIRPS	Precipitation	∼0.05° × 0.05°	Daily	1981–2018	Funk et al. (2015)
TAMSAT	Precipitation	4 km × 4 km	Daily	1983–2018	Maidment et al. (2017)

TRACK, which was developed to study extratropical storms tracks (Hodges, 1994, 1999) and has since been applied to tropical cyclones (Hodges et al., 2017) and tropical lows (Hurley & Boos, 2015). Hurley and Boos (2015) found that around 12.5 tropical lows formed each year in southern Africa, but their globally based approach did not provide detail on the nature of tropical lows over southern Africa. Other tracking algorithms have also been developed for similar purposes, and our results may depend on the choice of tracking method (Neu et al., 2013).

This study applies TRACK in the southern African context of region-specific land-based tropical lows in order to determine their fundamental properties and rainfall consequences. We examine the differences and similarities between the representation of tropical lows in three different reanalysis products and consider how this may reflect the true state of tropical lows in the real atmosphere. The following section discusses the data sets used in this study and elucidates the TRACK methodology. This paper then proceeds to address the following questions:

1. What are the frequencies, lifetimes, intensities, and preferred locations of the tropical lows which form and linger in southern Africa, as represented in reanalysis data sets (section 3)?
2. What control is exerted by ENSO on the interannual variability of tropical lows (section 4)?
3. Is there a link between tropical lows and TTTs on the synoptic time scale (section 5)?
4. What is the proportion of southern African rainfall that is associated with tropical lows, and how much interannual rainfall variance does this rain account for (section 6)?

Section 7 then examines how the results obtained from derived products such as reanalysis and gridded precipitation may reflect the true atmosphere and discusses implications for southern Africa. A sensitivity analysis of the tropical low detection thresholds is provided in Appendix A.

2. Data and Methods

This study uses three reanalysis data sets and two gridded precipitation products. The reanalysis products used are MERRA2, ERA-Interim, and the high-resolution run of ERA-5. The precipitation data sets considered are CHIRPS and TAMSAT. We elected not to use TRMM due to its shorter data availability. Table 1 summarizes the key features of each product.

2.1. Algorithm

The tracking algorithm described by Hodges (1994) was applied using a methodology based on Hodges et al. (2017), who use TRACK to identify tropical cyclones, as well as their antecedent and subsequent phases as tropical lows and tropical depressions. This was deemed appropriate since the southern African tropical lows are similar in spatial extent and magnitude to tropical lows which transition into and out from tropical cyclones. The only change made was to increase the lowest pressure level from 850 to 800 hPa, to take into account the high topography of southern Africa. This methodology created a superset of lows in southern Africa and the surrounding oceans, which contained all the land-based tropical lows as well as extratropical cyclones, ocean-based tropical lows, coastally trapped Kelvin waves, equatorial Rossby waves, and potentially spurious events.

More precisely, the tracking algorithm was applied as follows. First, an unweighted vertical average of 6-hourly instantaneous relative vorticity at atmospheric pressure levels 600, 700, and 800 hPa were averaged

vertically. The data were then smoothed to a horizontal resolution containing only the spherical harmonic wavelengths between 6 and 63, to remove the spurious effects of noise. A Sardeshmukh and Hoskins (1984) filter was applied to smooth the spectral cutoff. This step ensures that the same spatial scales are identified and smooths the data to make the tracking more reliable. All grid point vorticity minima within the domain of 0–100°E and 0–30°S with $\zeta < -5e^{-6}$ s^{-1} were identified and then refined using B-spline interpolation and steepest gradient descent minimization to identify off-grid minima. In the initial phase of tracking, these minima were linked together using a nearest neighbor method. The accuracy and realism of the tracks are then improved using an optimization scheme which minimizes a cost function of displacement distance and track smoothness based on adaptive constraints following the methodology of Hodges (1999).

To isolate the continental tropical lows, tracks that satisfied the following criteria were selected:

1. Tracks must spend at least one time step over the southern African mainland;
2. Track longevity must be at least 1 day;
3. The filtered vertical mean relative vorticity must satisfy $\zeta < -3e^{-5}$ s^{-1} in at least one 6-hourly time step;
4. There must be coincident cyclonic vorticity at 600, 700, and 800 hPa for a continuous 24-hr period;
5. The genesis location must not be in the Atlantic; and
6. The genesis location must be north of 25°S.

The second and third criteria are necessary to eliminate spurious events, and the sensitivity of the results of this paper to the threshold in the third criteria is considered in the sensitivity analysis (Appendix A). The fourth criterion ensures that the tracked lows are deep, eliminating heat lows, which are capped at middle levels by an anticyclone. Though coastally trapped Kelvin Waves are shallow features, they do sometimes have weak cyclonic vorticity aloft; thus, Criterion 5 is introduced to remove those that slip through the other criteria. We found that all the systems that formed in the Atlantic and then moved onto the continent were shallow coastally trapped Kelvin waves and not tropical lows. The sixth criterion eliminates extratropical cyclones.

In section 5, we consider the synoptic relationship between tropical lows and continental TTTs. Continental TTTs are identified as cloud bands with low daily outgoing longwave radiation using the MetBot algorithm developed by Hart et al. (2012), with centroids between 0°E and 40°E. A TTT was considered to be associated with a tropical low if the tropical low was located within 5° of the TTT axis on the day that the TTT formed.

2.2. Validation

No upper bound was placed on the strength of tropical lows, and so any tropical cyclone that made landfall onto the southern African mainland in the requisite time period would be counted as a tropical low. This provides the opportunity to validate our methodology against IBTrACS, the most complete global data set of tropical cyclones (Levinson et al., 2010), by confirming that the IBTrACS tropical cyclones that make landfall in southern Africa are detected by our algorithm. In the IBTrACS data set, 25 tropical cyclones met our criteria for landfall between November 1980 and March 2018. Notable cyclones in this data set included Tropical Cyclone Eline and Tropical Cyclone Bonita (Mudenda & Mumba, 1996; Reason & Keibel, 2004).

The tracked tropical low data sets for each reanalysis were compared to the IBTrACS data set. Two cyclones from different data sets were deemed to be the same event if their trajectories overlapped in time and the root-mean-square error (RMSE) between their locations at the overlapping times was less than 2.5°. In ERA-5, 24 cyclones were fully present and one (Severe Tropical Storm Lisette, February 1997) was missing. The RMSE averaged across all present cyclones was 0.9°. In ERA-Interim, 21 cyclones were fully present, 3 had a partial time overlap, and 1 (Severe Tropical Storm Astride, December 1999) was missing. Finally, in MERRA-2, 19 were fully present, 4 were partially present, and 2 (unnamed tropical depression of January 1998 and Moderate Tropical Storm Berobia of January 1986) were missing. The RMSE in overlapping times was 1.2° in both ERA-Interim and MERRA2.

To further validate the tracking algorithm, we compare the tracking results between the three reanalysis products. When tracks whose RMSE over the period of their overlap is less than 2.5° are deemed to be equivalent, 71% of ERA-Interim tracks, 65% of ERA-5 tracks, and 44% of MERRA-2 tracks are equivalent to a track in at least one other data set. We find that the track locations of low intensity events tend to diverge more than high intensity track events. When the RMSE threshold is increased to 4°, these proportions increase to 83%, 81%, and 62%. Note that with this methodology, a track in one reanalysis product may be equivalent to multiple tracks in another reanalysis product. Evidently, MERRA-2 shows less agreement than the other two
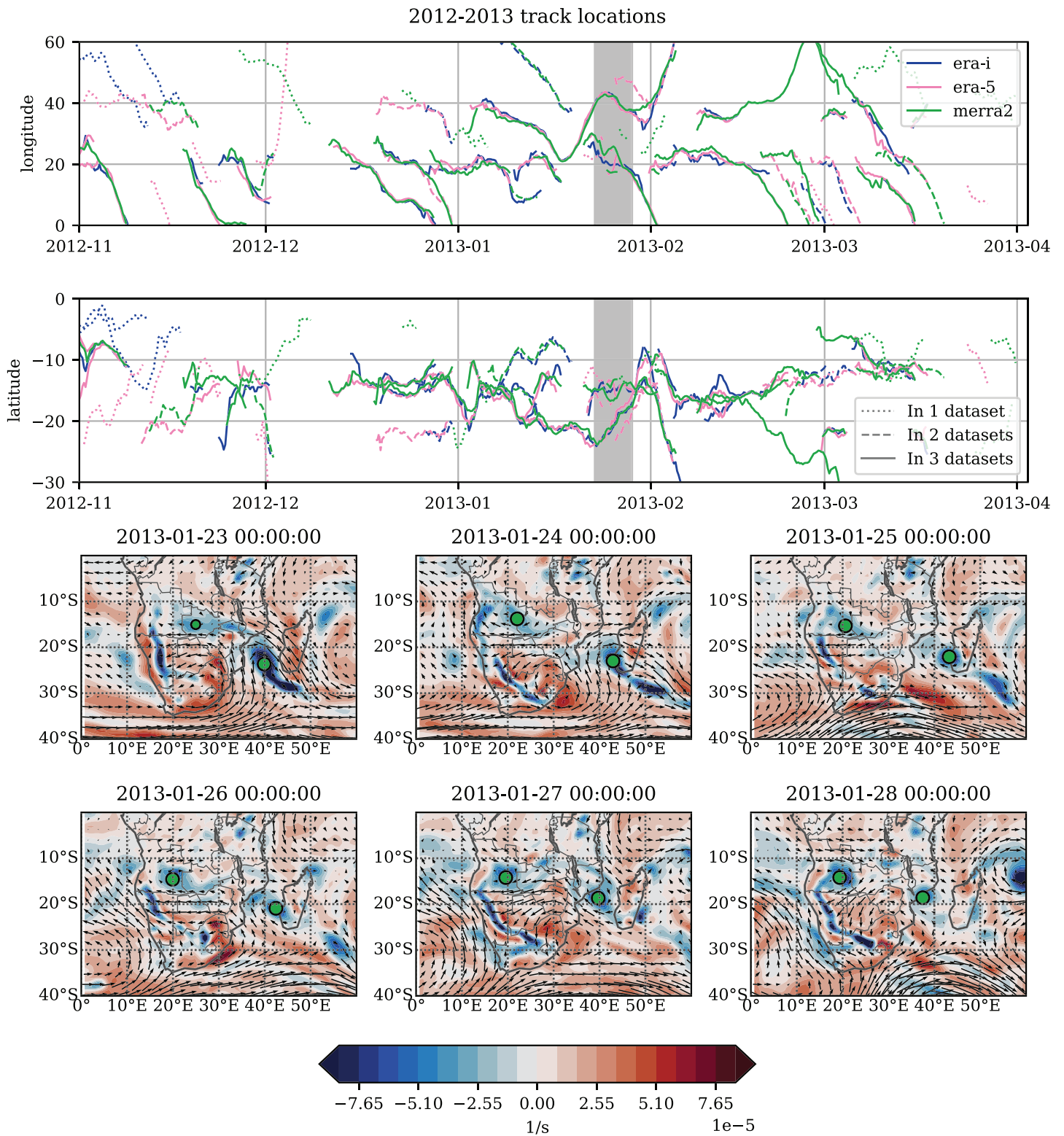
Figure 1. Top two rows: Hovmöller plots of track locations for a sample summer season (2015–2016). First panel: Longitude against time. Second panel: Latitude against time. Blue: ERA-Interim, pink: ERA-5, and green: MERRA-2. Solid lines denote tracks that have been identified in all three reanalyses, dashed lines show tracks identified in only two reanalyses, and dotted lines show tracks present only in one reanalysis data set. Black line: bottom row case study date. See text for methodology used to determine whether a track is present in more than one data set. Bottom two rows: ERA-Interim case study tropical low locations (dots) against 800-hPa vorticity and winds from 23 to 28 January 2013. The gray band in the upper panels indicate this time period. Smaller dots indicate weaker tropical lows.

reanalysis products. The top two rows of Figure 1 show Hovmöller plots of track locations in the 2012–2013 season, as a sample. Track matching is shown by line styles, using the methodology described above with the 4° RMSE threshold. From this, it can be seen that tracks tend to match each other quite well but sometimes diverge in different directions. Six of the isolated tracks that are not present in other reanalysis data sets are located over the oceans, only entering southern Africa for short intervals. It is possible that corresponding tracks were present in the other reanalyses but did not move over the southern African land mass.

The lower rows of Figure 1 shows the track locations from a sample week (23 to 28 January 2013) in ERA-interim, together with the 800-hPa winds and the nonfiltered relative vorticity. Two tropical lows were detected over southern Africa in each reanalysis on time period, one in Angola and the another in the Mozambique channel. Larger circles indicate the track location when the T63 filtered vorticity anomaly is larger than 3×10^{-5} s^{-1}, defined later as a threshold for strong tropical tropical lows. The cyclonic circulations around each strong tropical low centroid is clear, as is the associated vorticity. The wind fields and vorticity anomalies evolve slowly across the time period, and it is evident that the two tropical lows retain their coherence through time. The continental tropical low moves steadily westward from Zambia into Angola and intensifies, while the Mozambique channel event tracks north-westward, making landfall in Mozambique on the final day. A large, elongated cyclonic vorticity anomaly in Namibia is also evident in the vorticity map. This is the Kalahari heat low (Howard & Washington, 2018) and is a shallow feature, disappearing at 600 hPa. Based on the above analysis, we conclude that the track algorithm works acceptably well over southern Africa, and we proceed to examine its results in the following sections.

3. Characteristics of Tropical Lows

Applying the TRACK algorithm to the three reanalysis products lead to the identification of on average 44, 33, and 27 tropical lows per summer from November to March in MERRA-2, ERA-5, and ERA-Interim, respectively. These counts differ from that of Hurley and Boos (2015), due to differences in post-TRACK processing: we provide a minimum vorticity threshold rather than mean sea level pressure and specify a minimum duration of 1 day rather than 2 days. The specification of vorticity rather than sea level pressure is an important improvement since much of the interior of southern Africa lies above 1,500 m with the result that sea level pressure is fictitious given that lapse rates between 1,500 m and sea level can never be known. The months in which tropical lows were most common were December, January, and February. The following analysis describes key characteristics of the track locations and properties and contrasts the differences between the reanalysis products.

Tropical lows were identified across southern Africa and were most common between the latitudes of 10°S and 20°S, as shown in Figure 2, which shows monthly heat maps of tropical low locations in the three reanalysis products. In all reanalyses from December to February, the maximum number of tropical lows occurred along the 20°E longitude line, the locus of the Angola Low. This maximum was less pronounced in MERRA-2 than the other reanalyses, and the overall number of tropical lows in December and March was lower in ERA-Interim compared to both MERRA-2 and ERA-5. Meanwhile, there is a high degree of agreement evident in Figure 2 in the seasonal cycles, spatial patterns, and maximum frequencies between MERRA-2 and ERA-5. The mean tropical low latitude was 15.6°S in ERA-5, 15.7°S in ERA-interim, and 15.1°S in MERRA-2.

Figure 3 shows the genesis and lysis locations of tropical lows across the three reanalysis products, together with the individual genesis locations and track paths from one selected summer season (2006–2007). This season was chosen as a fairly typical tropical low year with neutral ENSO, for illustrative purposes only. From this figure it is evident that the vast majority of continental tropical lows form over land, as opposed to the Mozambique channel or the Indian Ocean. The latitude band around 13°S between 18°E and 30°E is a particularly strong genesis region in ERA-5 and MERRA-2, although not in ERA-Interim. There is a large lysis zone in the west of the domain at 0°E; however, this simply indicates tropical lows moving outside the tracking domain. In the top row of Figure 3, the increased latitudinal spread in ERA-Interim compared to the other reanalyses is again evident. Across the reanalysis products, 33.5% of tropical lows form in the Angola Low region (11–19°S, 14–25°E, consistent with Howard & Washington, 2018) and 23.5% lysis there. Meanwhile, the track density in the Angola Low region composes of 37% of the total track density.

Other characteristics of the tropical lows are presented in Figure 4. It is apparent from the top right panel that the most common duration of a tropical low is 4.5 days, although some last up to a month. Due to the
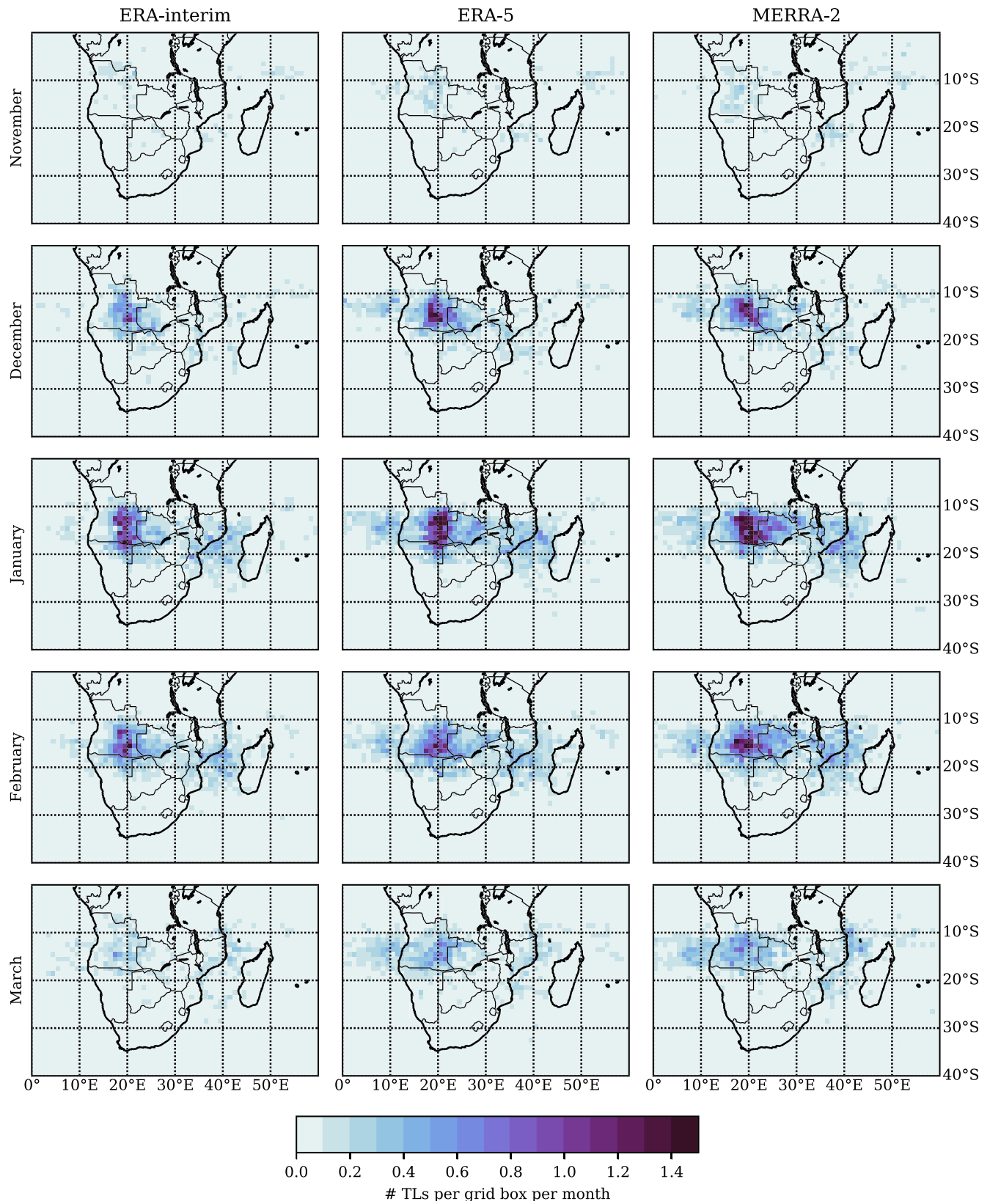
Figure 2. Monthly track density in each reanalysis product of tropical lows (number of incidents per $1° \times 1°$ grid box per year). Left column: ERA-Interim. Middle column ERA-5. Right column: MERRA-2. Rows show different months from November to March, as labeled. The strong vorticity threshold ($-3e^{-5}s^{-1}$) has been applied. TL = tropical low.
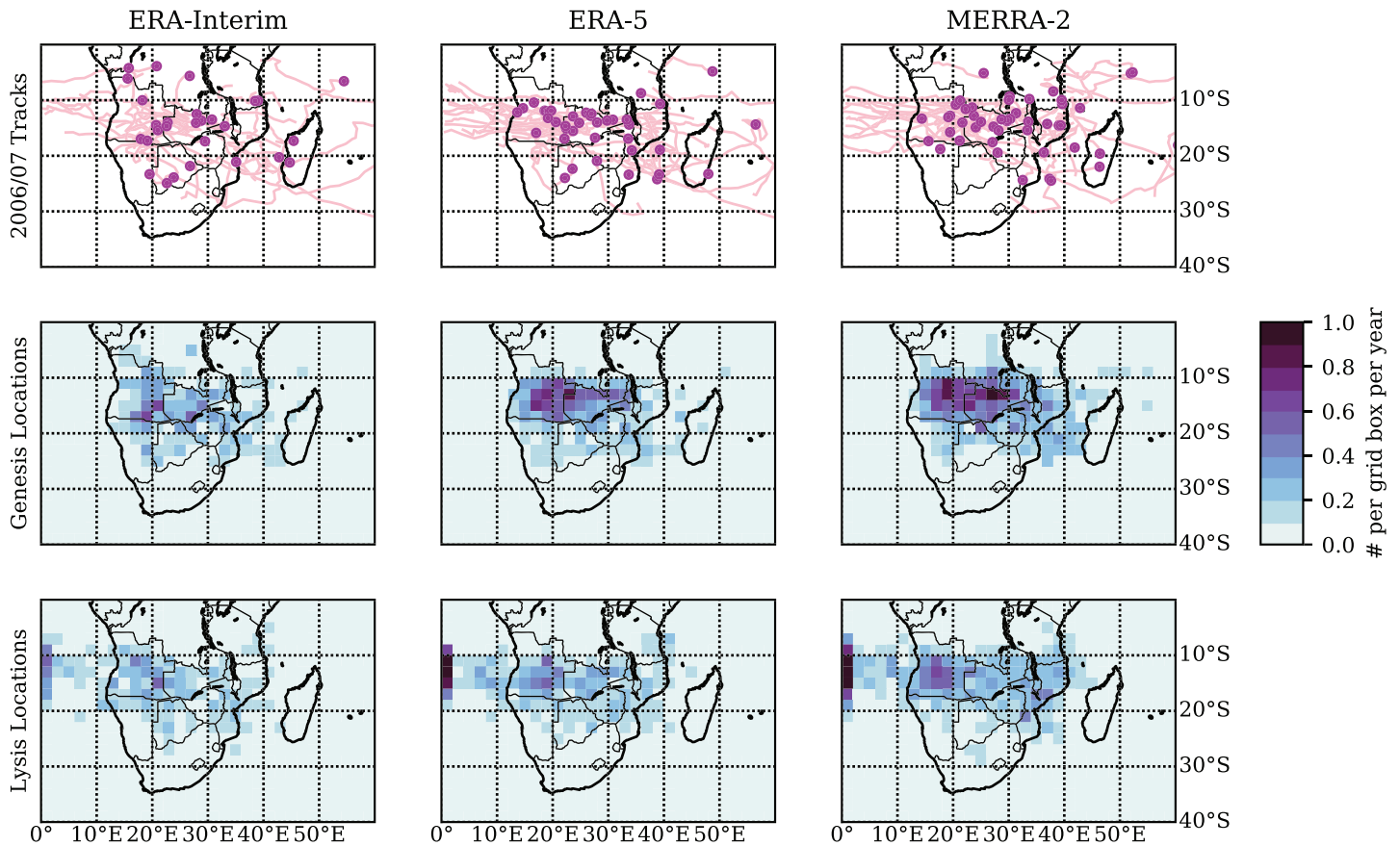
Figure 3. Track feature locations for three reanalysis products. Top row: Track paths (pink lines) and genesis points (purple dots) for one selected summer season (2006–2007). (middle row) Genesis locations (number of incidents per 2° × 2° grid box per year). Bottom row: Lysis Locations (number of incidents per 2° × 2° grid box per year). Left column: ERA-Interim. Middle column: ERA-5. Right column: MERRA-2.

skewness of the distributions, the mean longevity is 7.5 days. In MERRA2, this long tail of the distribution is reduced compared to the other reanalyses, and so although MERRA2 has more tropical lows per year than ERA-5, the total number of tropical low days in the two data sets is roughly equal. This is likely be due to some tropical lows in MERRA-2 decaying and then reforming and so being counted twice as compared to in ERA-5 where they may have persisted as the one system. The predominant track direction hypothesized from the tracks in Figure 3 is confirmed in the bottom right panel, showing that the most common track direction is west. The left and center panels show frequency, intensity, longevity, and eastward velocity as functions of longitude.

The spike in frequency at the Angola Low locus is again evident in the frequency plot in Figure 4. This comes with an increase in intensity and longevity at the same location. The increase in longevity explains the differences in the peaks at 20°E between Figures 2 and 3: tropical lows to the east of 20°E do not last as long as those at 20°E. Note that the longevity in the lower left panel is calculated at each longitude as the average longevity of each track that exists at that longitude at some time. If a track stays at one longitude for more than one time step, then it is multiply counted, and if it moves between longitudes, then it is included in the average at all these locations. The sudden drop of in frequency to the west of the 20°E meridian is explained by the bottom center panel: An increase in the mean track velocities of the tropical lows means from 2 to 4 m/s ensures that tropical lows move swiftly away from the zone between 8°E and 18°E and out into the Atlantic ocean. Over the Indian Ocean between 40°E and 60°E, mean tropical low intensity is steady at around $4e^{-5}$ s^{-1}, which then decreases as tracks move inland, before recovering in Angola. The longevity of tracks in the Indian Ocean declines as tracks reach the coast, which may be a selection effect: Tracks that
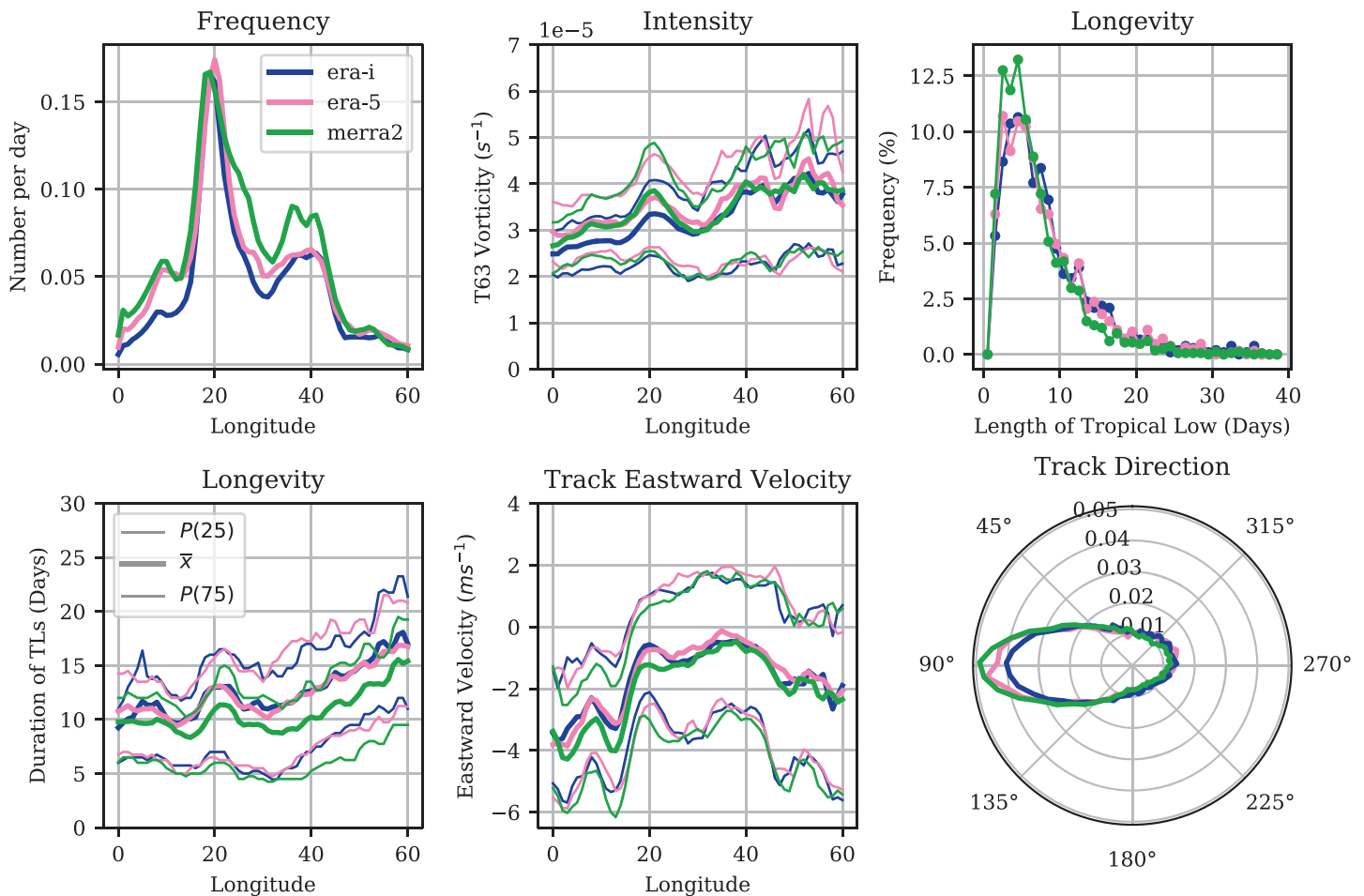
Figure 4. Top left: Probability that a tropical low will be present at a given longitude on a given day over the main tropical low season. Top center: Average filtered vorticity at center of each tracked low at each time step by longitude. Top right: Overall distribution of tropical low lifetimes. Bottom left: average track duration at each time step as a function of longitude. Bottom center: Average zonal velocity of track motion at each time step by longitude. Bottom right: Polar distribution plot of track direction in degrees. Thinner lines, when present, indicate the interquartile range. Line colors indicate reanalysis product, with dark blue: ERA-Interim, pink: ERA-5, and green: MERRA-2.

exist at 60°E must exist for a longer duration in order to travel westward and meet the criteria of making landfall onto southern Africa.

4. Interannual Variability

In the previous section, we established that tropical lows occur regularly in southern Africa in the austral summer and thus are a significant feature of the local climatology. This raises the question of how they vary from year to year and the potential causes of this variability. This question is particularly pertinent due to the high degree of rainfall variability in southern Africa and the potential contribution of tropical lows to southern African summer rainfall, which will be addressed in section 6. In this section, we quantify and compare the interannual variability of the incidence frequency of tropical lows in the three reanalysis products, characterize the relationship between tropical lows and ENSO, and identify a link between the tropical easterly jet (TEJ) and seasons with high tropical low activity.

In order to obtain a sensible measure of the interannual variability of tropical low occurrence, we considered the number of days in each year featuring tropical lows centered over land with $\zeta < -3 \times 10^{-5}$ s^{-1}. This metric creates a good sample of the number of days with strong lows in a season. The top panel of Figure 5 shows a time series of this metric over the years in the study period for each reanalysis product. The lesser number of tropical lows in ERA-Interim compared to the other data sets is apparent from this figure. The correlation coefficients between pairs of reanalyses during their overlaps were 0.72, 0.73, and 0.77 for
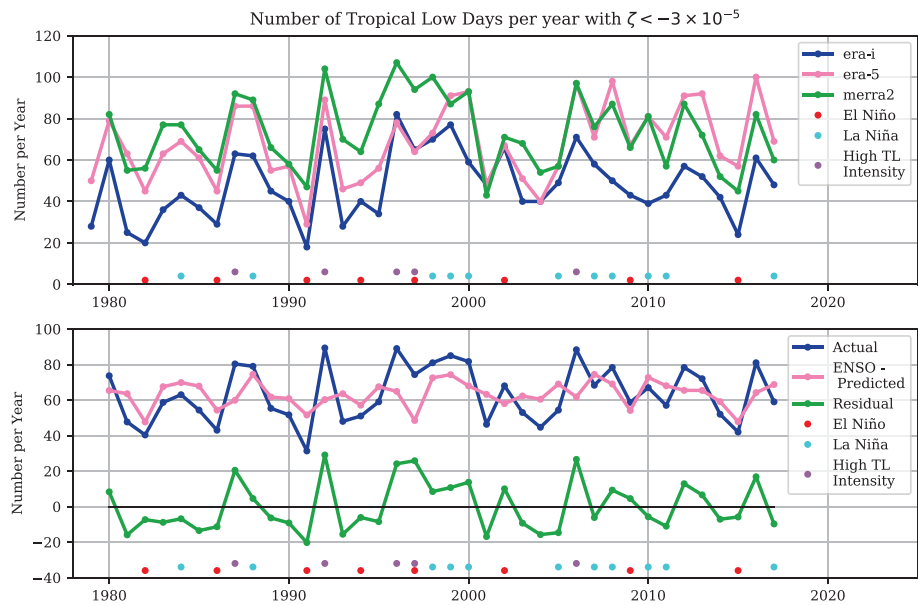
Figure 5. Upper panel: interannual variability of number of strong ($\zeta < -3 \times 10^{-5}$) continental tropical low days per year in each reanalysis product. Colors indicate reanalysis product. Lower panel: average number of strong continental tropical low days per year across reanalyses (dark blue), prediction of the blue line based on a regression onto the Niño 3.4 sea surface temperature (SST) index (pink) and the residual of this regression (green). The dots at the bottom of the panels indicate the years of the composites used in Figures 7 and 12: red for El Niño, light blue for La Nin¨a, and purple for the high TL intensity composite. TL = tropical low.

pairs [MERRA2, ERA-5], [ERA-5, ERA-Interim], and [MERRA2, ERA-Interim], respectively. The statistics of these relationships will be further explored later in this section using composites.

The ENSO is an important driver of interannual variability in tropical lows, with more tropical low days in the La Niña phase and fewer in the El Niño phase. The correlation R values were -0.48, -0.38, and -0.38 between the interannual tropical low index described above and the JFM Niño 3.4 sea surface temperature (SST index, for ERA-5, ERA-Interim, and MERRA2, respectively. All values are significant at the $p = 0.05$ level. The lower panel of Figure 5 shows the average number of tropical low days across reanalyses per year compared to the predicted number of tropical low days based on regression onto the Niño 3.4 SST index (December, January, and February). It is evident that there is a strong underprediction in 1987–1988, 1992–1993, 1996–1997, 1997–1998, and 2006–2007. This is consistent with the results of Reason and Jagadheesha (2005), who found that the strong Angola Low was present during the 1997–1998 El Niño and linked this to the lack of materialization of an El Niño linked drought in this year.

For each month between November and March, the interannual monthly average number of tropical lows across the three reanalyses was calculated and regressed on the Niño 3.4 SST index 3-month average centered on that month. The result of this regression was significant at a $p < 0.05$ level for December, January, February, and March, though not for November. Based on these regressions, two composites of months were created: the first where the residual of the above regressions was above 8.2 tropical low days per month and the second where the residual was smaller than -8.2 tropical low days per month. The value 8.2 was chosen as $1.5 \times \sigma$, where σ is the standard deviation of the residuals across all five regressions. The resultant months in the first composite were as follows: March 1988, February and March 1993, February 1995, February 1997, January 1998, March 2000, March 2003, January 2007, December 2008, and January 2013 and January 2015. The second composite contained January 1985, December 1988, February 1992, December 1993, December 1994, January 2000, February 2005, February 2008, February 2011, and February 2012 and February 2015. These composites are designed to extract the interannual mode of variability of tropical lows that is independent from ENSO. The full wind vectors at 800 hPa are shown in Figure 6. The Angola Low is much stronger in the composite with more tropical lows than that with less tropical lows, by construction.

Figure 6 also shows the monthly anomalous zonal winds at 200 hPa for the two composites, with full winds contoured in blue. From this it is apparent that the TEJ is anomalously strong over central and southern
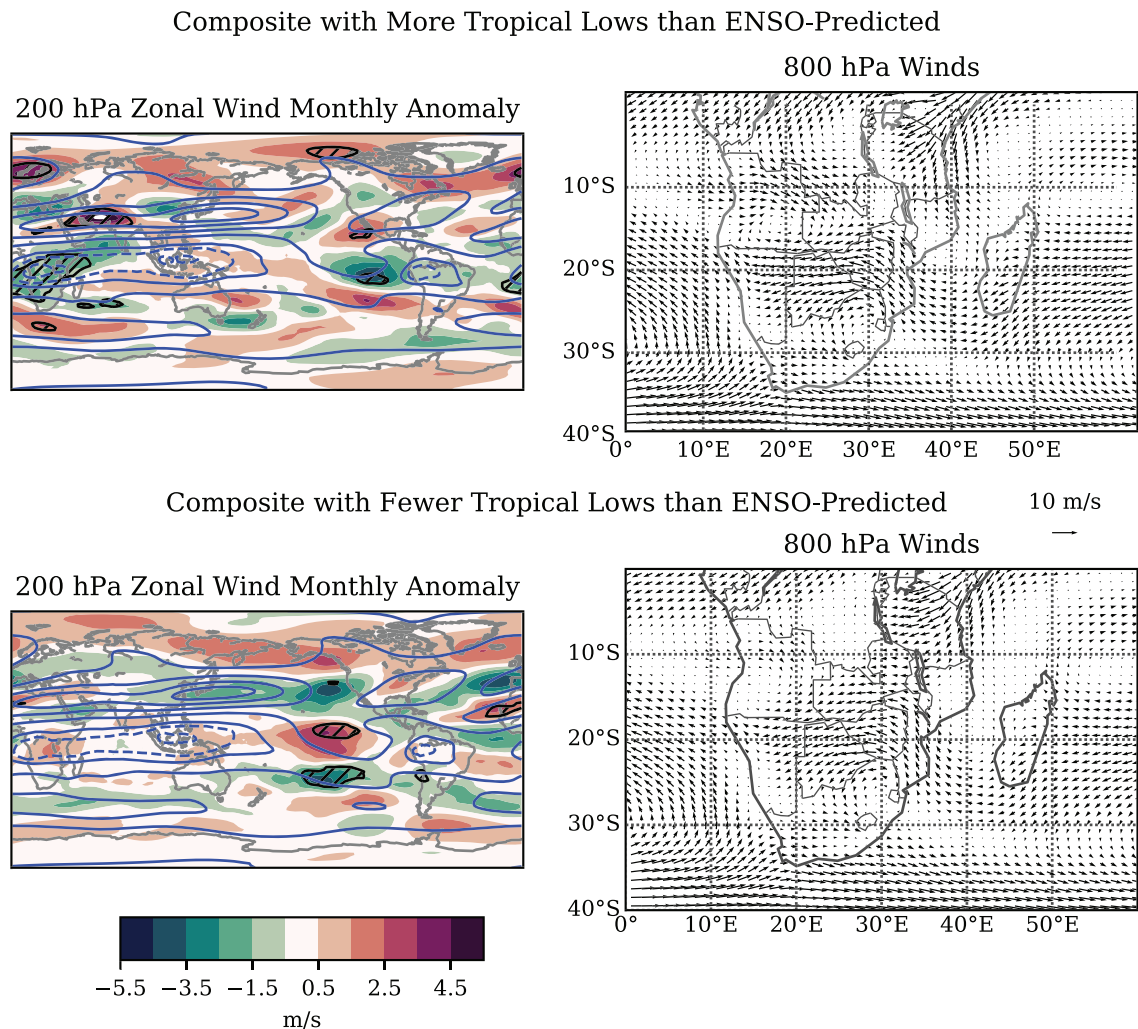
Composite with More Tropical Lows than ENSO-Predicted

Figure 6. Stronger-than-ENSO (top row) and weaker-than-ENSO composites (bottom row). Left: 200-hPa MERRA-2 zonal winds with colors showing the wind anomaly (m/s), blue contours: full composite wind speed (negative contours dashed with 5-m/s contour intervals, positive contours solid with 15-m/s contour interval). Shaded regions: significant at a $p < 0.01$ level. Right: full 800-hPa wind vectors. ENSO = El Niño–Southern Oscillation.

Africa in the first composite. This result is significant at the $p < 0.01$ level. It is slightly weaker than average in the second composite, although this result is not significant at the $p < 0.01$ level. Although these composites were designed to study a mode of variability that was distinct from ENSO, there remained an ENSO signal in the composites, with the strong composite having a slight overall El Niño signal and vice versa. This is in part due to the inclusion of the 1997–1998 El Niño in the strong composite. This led to significant wind anomalies over the western Pacific in Figure 6. However, when the Niño 3.4 signal was removed from the 200-hPa winds, the TEJ signal remained significant and the western Pacific signal did not (not shown).

Therefore, the strength of the TEJ over Africa appears to be linked with the interannual variability of tropical low days, in a manner that is independent from ENSO. However, this does not imply causation and the direction of any causation that may exist is unknown. It is possible that increased upper level wind speeds may make the formation of tropical lows more likely. However, an increase in tropical low activity would provide a heat source in the upper atmosphere, which may accelerate the TEJ.

To examine the spatial distribution of the interannual variability, three seasonal composites were considered. The first consisted of five El Niño years with Niño 3.4 SST anomalies greater than 0.8 K and are indicated by red dots in Figure 5. The second consisted of five La Niña years with Niño 3.4 SST anomalies below -0.8 K, indicated in Figure 5 by light blue dots. The final composite, labeled as the high TL intensity composite, contained the years described above where the annual tropical low strength was significantly underpredicted
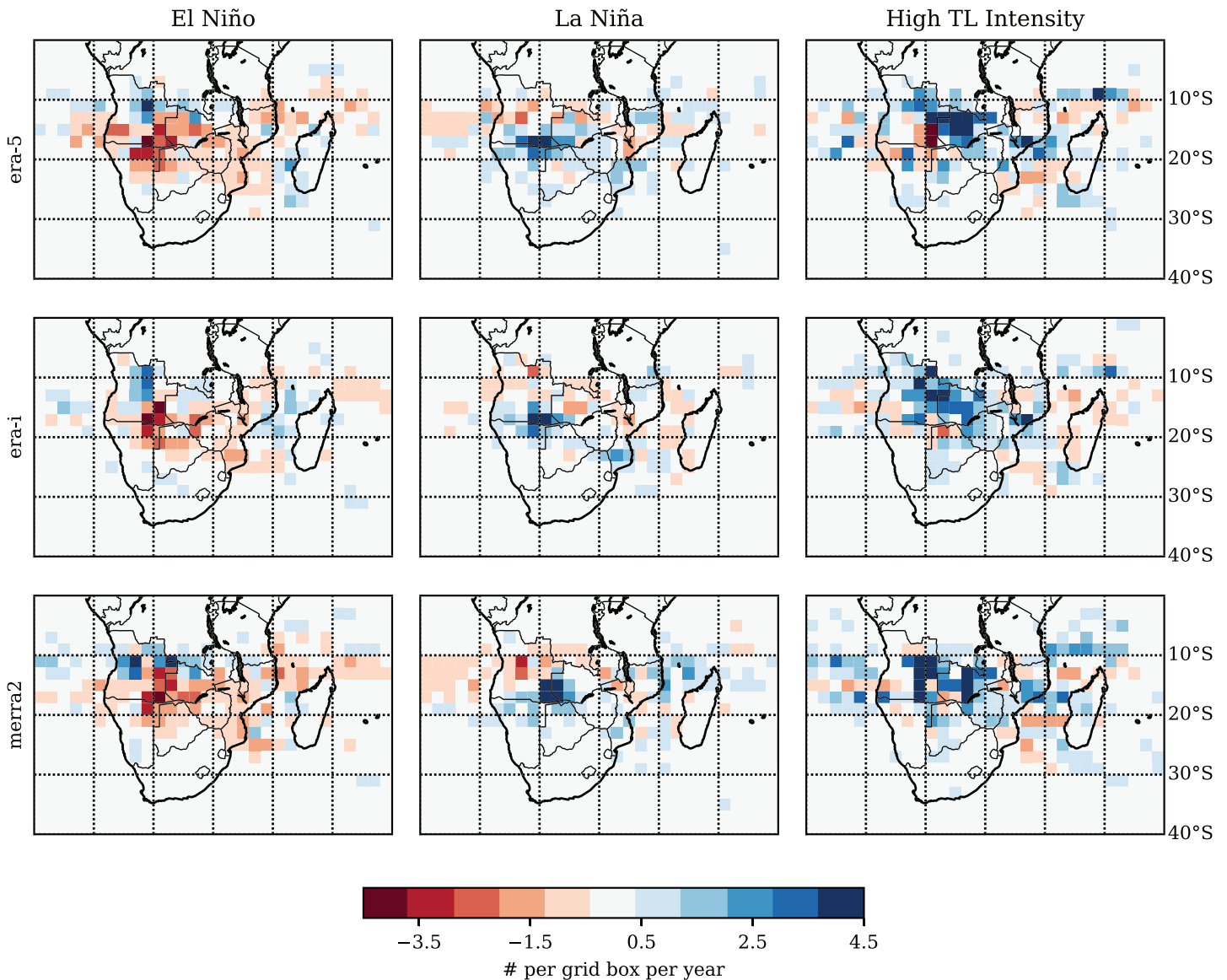
Figure 7. Annual anomalous track density for (left) El Niño composite, (center) La Niña composite, and (right) the high tropical low intensity composite. Rows indicate the reanalysis product used—top row: ERA-Interim, middle row: ERA-5, and bottom row: MERRA2. The strong vorticity threshold ($-3e^{-5} s^{-1}$) has been applied.

by the ENSO regression and is shown in purple dots. The 1997–1998 season was included in both the first and the third composite because a strong El Niño and a strong positive residual were both present during that season.

Figure 7 shows the difference between the climatological heat maps and the composite heat maps for each case. In the El Niño composite, there is a slight northward shift in the preferred track location, as well as an overall decrease in the number of tropical lows. In the La Niña composite, there is an overall increase and a southward shift. This is consistent with the general behavior of El Niño reducing precipitation in subtropical southern Africa and vice versa for La Niña (Lindesay, 1988). The northward and southward shifts of the composite mean track centroids compared to the climatology were significant at a $p = 0.05$ level, using a one-sided Welsh's t test. These t tests were performed using all latitudes of tropical lows over land at time steps where the filtered vorticity satisfied $\zeta < -3e - 5\ s^{-1}$ and used the total number of tropical lows (as opposed to the number of tropical low days) as the degrees of freedom. During La Niña, the mean tropical low latitude over land shifted 0.5° further south compared to the climatological mean in each reanalysis product. During El Niño, the shift was 0.8° north in ERA-5 and MERRA-2 and 1.0° north in ERA-Interim.

In the final composite, the increase in tropical low frequency occurs throughout the domain and no clear shift in preferred location is apparent.

A statistically significant overall increase in the number of tropical low days a year is observed at the $p = 0.05$ level during La Niña phase in ERA-5 (12 days/year) and ERA-interim (9 days/year) but not in MERRA-2. A significant overall decrease is observed in the El Niño phase in ERA-5 only (14 days/year). However, if 1997–1998 is removed from the ENSO composite, the decrease becomes significant for every reanalysis product. The high TL intensity saw a significant increase in all three reanalysis products, with increases of 16, 24, and 27 days a year.

5. Links and Limitations Between Angola Tropical Lows and TTTs

It has often been hypothesized that the genesis of TTTs is linked to the behavior of the Angola Low (Todd & Washington, 1999). Since the Angola Low is the climatological result of the synoptic anchoring of tropical lows in the Angola region, it is reasonable to ask whether there is a link on the synoptic time scale between TTTs and Angolan Tropical Lows (ATLs). In this section, we investigate whether there is a synoptic link between these two classes of events.

If TTT and ATL events were completely unrelated on a daily time scale, then according to the definition of statistical independence, the probability of TTTs that form on an ATL day would be equal to the product of the probability that the day is an ATL day with the probability that a TTT would form on that day. Since ATL and TTTs possess different seasonal cycles, this is equivalent to saying that if TTT and ATLs were completely unrelated, then the proportion of days at a given time of year in which of TTTs that form on during an ATL would be equal to the product of the proportion of days that are ATL days with the proportion of days on which a TTT forms, at this time of year, that is,

$$P(TTT \cap ATL)_t = P(ATL)_t \times P(TTT)_t \quad \forall t \iff \text{TTT, ATL are independent}$$

Conversely, if ATLs caused TTTs, then $P(TTT \cap ATL)_t$ would be greater than $P(TTT)_t \times P(ATL)_t$ for some time of year t.

To determine the interdependence of ATLs and TTTs, Figure 8 compares the predicted probability of TTTs forming on ATLs under the assumption of independence with the observed coincidences of these events. The existence of the ATL has been determined using the three reanalysis products. The top left panel of Figure 8 indicates the seasonal cycle of the TTT formation (black) and ATL occurrence (colored). The right panels indicate the seasonal cycle of the proportion of days with formation of TTTs during ATLs (colored solid lines) and the theoretical prediction of this metric under the assumption that TTTs and ATLs are independent (black line). The dashed line shows the proportion of these events where the axis of the TTT came within 5° of the ATL. In all cases, the probabilities are almost indistinguishable. This implies that the presence of an ATL does not alter the likelihood of TTT formation at any time of the year.

The bottom left panel of Figure 8 shows PDFs of the minimum separation distance between the axes of TTTs and the centroids of ATLs when the two events occur on the same day. In all cases the frequency decreases with the distance and 80% of the separation distances are smaller than 5° across reanalysis products. This distance has been chosen as the cutoff distance at which TTTs and ATLs will appear to be synoptically linked (see Appendix A for a sensitivity analysis). Thus, although ATLs do not appear to make TTTs more probable, when TTTs form during ATLs, they do appear to interact with the tropical convection associated with the ATL.

The interannual and intermonthly statistical correlations between the number of TTTs and Angola tropical lows in each year in each reanalysis are given in Table 2. The correlation between the number of TTTs and the number of tropical lows in each summer season (December, January, February, and March, DJFM) from 1979 to 2012 are of order 0.4 and are significant at the $p = 0.05$ level. The period of December to March was chosen because it is the intersection of peak TTT season with peak ATL season. To consider the relationship at a monthly time scale, time series of number of ATLs and TTTs, respectively, in each January, February, March, and December between 1979 and 2012 were compared. In this case, the correlation decreased and became insignificant. In order to account for the differing seasonal cycles of TTTs and ATLs, the climatological mean number of events in each month was removed from the time series before correlating. This
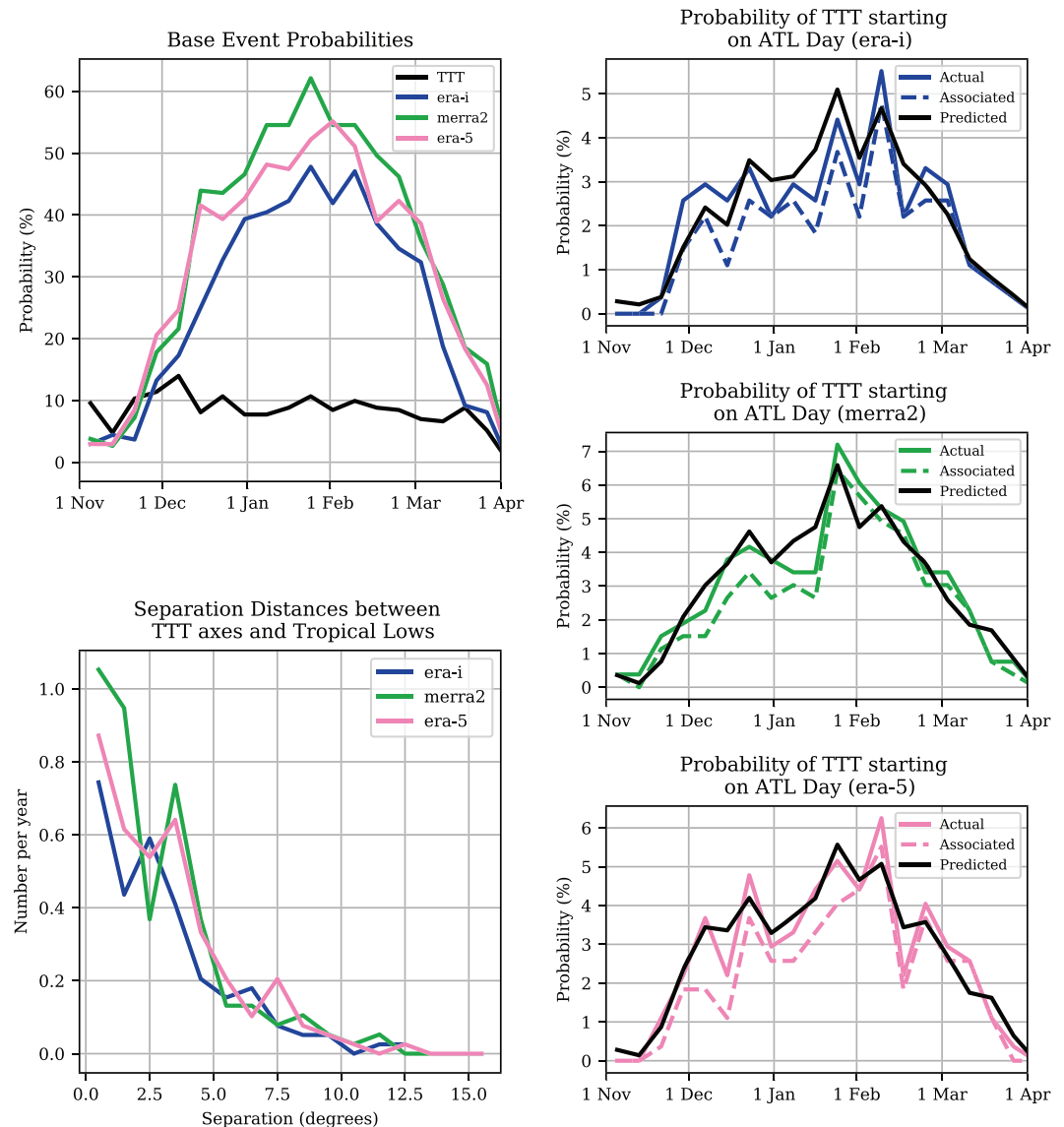
Figure 8. Seasonal cycles of probabilities of Angola tropical lows nd TTTs, together with separation distances between coincident events. Top left: probability of TTT events beginning (black line) and Angola tropical lows occurring (colored lines) on a given day. Bottom left: Separation distance between Angola tropical low centroid and TTT axes on days where Angola tropical lows and TTTs both occur. Right: Probability of TTT and Angola tropical lows occurring on the same day. Solid colored lines: observed coincident events, dashed colored lines: observed coincident events with separation distance <5°, black: predicted probability of coincident events under the assumption of statistical independence. TTT = Tropical Temperate Trough; ATL = Angolan Tropical Low.

suggests that the relationship between TTTs exists on an interannual time scale but not at higher temporal resolution.

The following three scenarios are all logically consistent with this result:

1. There is an independent phenomenon, which operates on an interannual or annual time scale, which modulates the frequency of both TTTs and ATLs. The above interannual variability analysis suggests that ENSO and the TEJ are candidates for this scenario.
2. In some years, the unusually persistent presence of ATLs modifies the large-scale atmosphere, for example, by enhancing the Hadley Circulation and shifting the southern subtropical jet northward, causing TTTs to become more frequent.

Table 2
Interannual Correlation Statistics Between the Number of TTTs and Angolan Tropical Lows in Each Time Period

Timescale	Statistic	ERA-5	ERA-Interim	MERRA
Seasonal	*R*	0.40	0.48	0.38
	N	32	32	32
	S.E.	0.026	0.030	0.030
	P value	0.025	0.0055	0.030
Monthly	*R*	−0.12	−0.03	−0.07
	N	128	128	128
	S.E.	0.011	0.012	0.011
	P value	0.195	0.750	0.410

Note. Top section: time periods are aggregated December, January, February, and March seasons. Bottom section: time periods are months (December, January, February, and March only).

3. In some years, the southern subtropical jet exists further north than usual, and this leads to more frequent ATL occurrences. However, this result provides more evidence against the existence of a direct causal synoptic link between the ATLs and TTTs.

Although we have established that there is no synoptic causal link between ATLs and TTTs, a quarter of summer TTTs events occur in association with ATLs, with a minimum separation distance smaller than 5° between the TTT axis and the ATL center. Therefore, we next examine the influence that an ATL along the axis of a TTT has on the precipitation of that TTT. In the following, a TTT is considered to be associated with an ATL if the TTT axis comes within 5° of the ATL center.

The top row of Figure 9 shows composited anomalous precipitation (colors) during TTT events, TTTs associated with ATLs and ATL events. Data have been drawn from MERRA-2 and CHIRPS only, as similar results were obtained when ERA-Interim, ERA-5, and CHIRPS were considered. From this it can be seen that the TTTs associated with ATLs feature more seasonally anomalous rainfall than average TTTs. The bottom row of Figure 9 compares this to the linear superposition of anomalies associated with the composites of the TTT-only and ATL-only days. The linear superposition is not vastly different to the rainfall on combined days, as demonstrated by panel e, which shows the difference between the combined event rainfall and the linear superposition. A Welch's *t* test, applied to test whether the data displayed in panel e was significantly different from zero, was unable to reject the null hypothesis at any grid cell after the false discovery rate was controlled for using $\alpha_{FDR} = 0.05$ (Wilks, 2016). This suggests that the increased precipitation from TTTs associated with tropical lows, as compared to TTT only events, may simply be the rain that would have fallen from the tropical low anyway. Therefore, this analysis has been unable to distinguish combined event rainfall from the superposition of ATL rainfall with TTT rainfall. This casts doubt further on the existence of a synoptic link between TTTs and ATLs, although the tests applied were not formulated to prove the null hypothesis.

6. Precipitation Associated With Tropical Lows

In many regions across the low latitudes, tropical lows are an important feature of local climatologies because of their contribution to annual precipitation. In southern Africa, understanding precipitative processes is particularly pertinent due to the high degree of interannual rainfall variability. In this section, we determine the proportion of rainfall that may be attributed to tropical lows in southern Africa and the degree to which tropical low variability controls the overall rainfall variability. In order to determine the precipitation contribution of tropical lows, we need a means to attribute rainfall to tropical low events.

Figure 10 illustrates the methodology used to attribute rainfall to tropical lows. In the first column, the CHIRPS and TAMSAT rainfall on an example tropical low day is shown. In CHIRPS, a large patch of rainfall exceeding 40 mm/day that is located to the northeast of the tropical low is present, and it is highly plausible that this rainfall is associated with the tropical low. The high-intensity blob is contained within 5° of radius of the tropical low centroid. Other rainfall regions are present further afield, but it is unclear whether or not
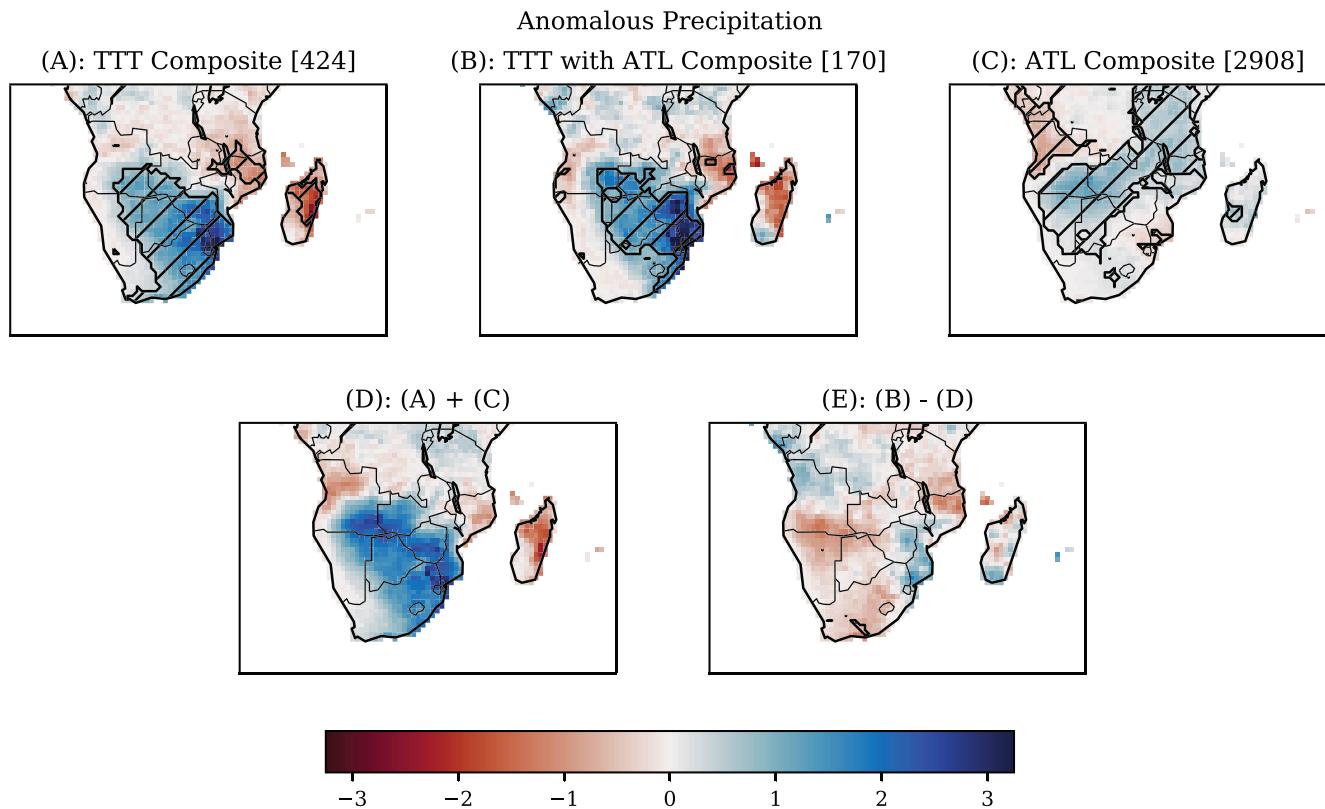
Anomalous Precipitation

Figure 9. Upper row: Precipitation anomalies (mm/day) associated with: (a) TTTs, (b) TTTs coincident with Angola tropical lows with separation distances 5°, and (c) Angola tropical lows. Shading indicates where the result is significantly different from 0 at the $p < 0.05$ level. Numbers in the top right indicate the sample size. Precipitation anomalies are calculated with respect to the climatological daily mean of CHIRPS, smoothed with a 2-week running mean, and composited on days of TTT and/or Angola tropical lows as described in the text. Lower row: linear combinations of the upper panels. (d): The linear superposition of the TTT anomaly and the Angola tropical low anomaly. (e). The difference between the anomaly due to combined events and the linear superposition from (d). TTT = Tropical Temperate Trough; ATL = Angolan Tropical Low.

they are associated with the tropical low. The picture in TAMSAT is similar, although the central rain patch beside the tropical low is less intense. Based on this case study, we consider composites of rainfall centered on the tropical low centroids.

The second column of Figure 10 shows the composite anomalous rainfall footprint of tropical lows across data sets, shifted so that the center of the low is at the plot origin. The climatology used to create the rainfall anomaly is the smoothed interannual daily rainfall climatology. Since the rainfall data sets were both daily and the tracks were computed every 6 hr, the composite was constructed by identifying the closest grid cell to the 12 p.m. UTC location of each tropical low on each day and shifting that grid cell to the origin. The composite mean was calculated using the tracks from the three reanalysis products separately, and then the three resultant composites were averaged together. It is evident that the rainfall is increased at the center of and to the east of the low. Since tropical lows move predominantly in a westward direction, the rain to the east of the low is most likely a result of the low having been in that location the day before. The positive anomaly is largely contained within a circle of 5° radius around the center of the low. Therefore, we attribute all rain which falls within 5° of a tropical low as associated with that tropical low. This radius is consistent with many previous studies of tropical lows and tropical cyclones (e.g., Dare et al., 2012; Khouakhi et al., 2017; Lavender & Abbs, 2013). The spatial distribution of the composite anomalies in the three separate reanalysis products was all the same (not shown), but the intensity varied slightly between the reanalyses: For example, the CHIRPS maximum composite anomaly was 5.2 mm/day in ERA-5, 5.0 mm/day in ERA-interim, and 3.8 mm/day in MERRA-2.

Based on the attribution methodology described above, between 30% and 70% of precipitation across the tropical edge (16–22°S) from November to February was associated with a tropical low. This is demonstrated in the third column of Figure 10, which shows a map of the proportion of rainfall attributed to tropical lows.
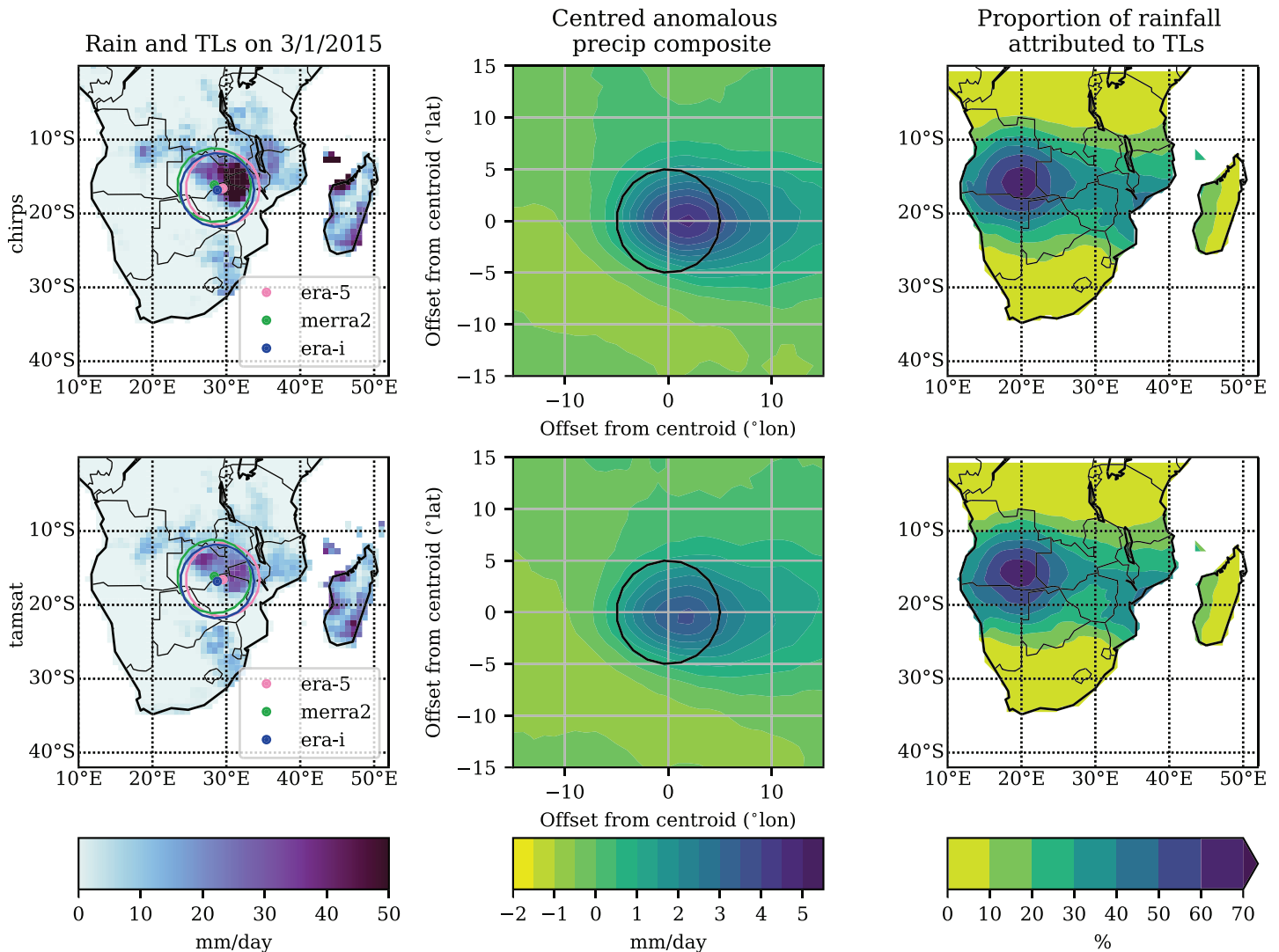
Figure 10. Rainfall attribution. Top row: CHIRPS. Bottom row: TAMSAT. The left column shows rainfall on a sample tropical low day (3 January 2015), with the centroid of the tropical low in each reanalysis product shown as a pink, green, or blue dot for ERA-5, MERRA-2, and ERA-Interim. A circle of 5° radius is shown around each centroid in the same color. The middle column shows a composite of climatologically anomalous rainfall centered around tropical low centroid (mm/day), averaged across all days and the three reanalysis products. Black circle indicates a radius of 5° around the tropical low centroid. The right column shows the proportion of November, December, January, February, and March rainfall which falls within 5° from a tropical low centroid. The proportion was calculated independently for each reanalysis product and then averaged. TL = tropical low.

By averaging over the tropical edge latitude band, we found that 31% of rainfall in this region was attributed to tropical lows. In each case, the maximum occurs in southeast Angola, and most of the rainfall occurs between 10 and 25°S. Again, the spatial structure was consistent across reanalysis products. Overall, there is a lesser fraction of rainfall contributed by tropical lows when ERA-Interim was used to identify the tropical lows, as compared to the other two reanalyses (not shown). The maximum rainfall contributed by tropical lows was approximately 10% lower in ERA-Interim than the other two products. This was likely due to the smaller number of tropical low days identified in ERA-Interim. There is a good agreement between the two gridded rainfall products.

Interannual rainfall variability is of key concern in southern Africa, and the tropical edge is one of the regions where variability is highest. This raises the question: How much of the variability in this region is variability in tropical low rainfall, and how much derives from other forms of precipitation?
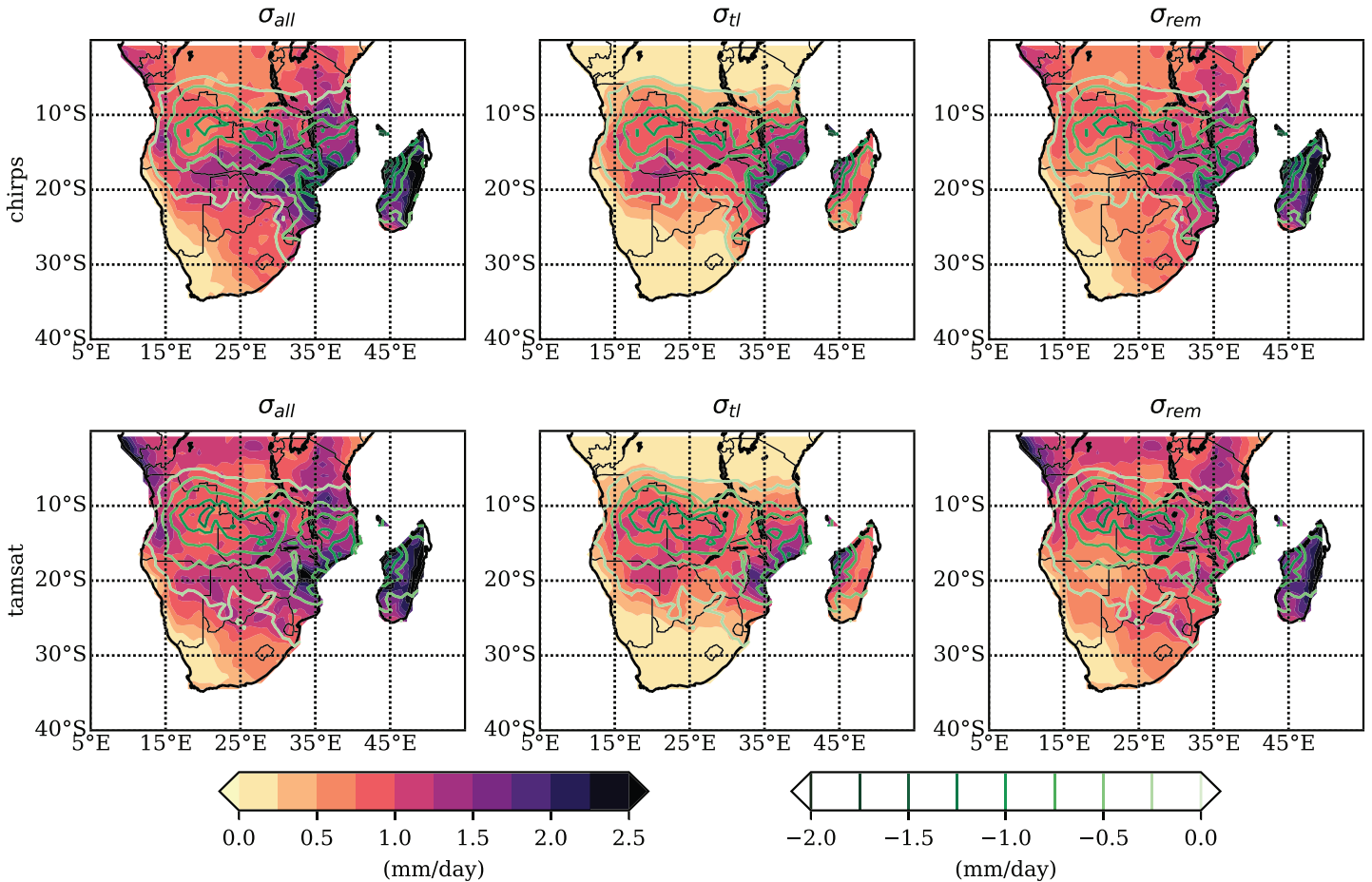
Figure 11. Interannual rainfall variability attributed to tropical lows. Top row: CHIRPS. Bottom row: TAMSAT. Column 1: interannual standard deviation of total November, December, January, February, and March (NDJFM) precipitation. Column 2: interannual standard deviation of NDJFM precipitation attributed to tropical lows. Column 3: interannual standard deviation of remaining NDJFM precipitation not attributed to tropical lows. The green contours indicate the interannual covariance between tropical low rainfall and other rainfall. For clarity, only nonpositive contours of covariance are marked. Each quantity was calculated independently using tracks from ERA-interim, ERA-5, and MERRA-2 and then averaged over the three reanalysis products.

The first column of Figure 11 shows the interannual standard deviation of November, December, January, February, and March precipitation across southern Africa in CHIRPS and TAMSAT, respectively. The variability of the tropical edge can be seen very clearly in CHIRPS, as a zonal line of high standard deviation near 18°S. In TAMSAT this is slightly less distinct, but the standard deviation is high between the latitudes between 15°S and 25°S. The interannual variability can be decomposed as follows:

$$\sigma^2 = \sigma^2_{tl} + \sigma^2_{rem} + 2 \times \mathrm{cov}(P_{tl}, P_{rem})$$

In the above equation, σ, σ_{tl}, and σ_{rem} are the standard deviations of the seasonal total precipitation, precipitation from tropical lows, and remaining precipitation, respectively, and the "cov" term is the covariance of the seasonal precipitation from tropical lows and the remaining precipitation. This decomposition is shown in the remaining columns of Figure 11. The green contours on Figure 11 show the negative covariance values. Where the covariance is positive or has a relatively low negative value, the interannual variability of tropical low rainfall has a strong control on the total interannual variability.

In the southern tropical edge region, the variability in the rain from tropical lows is high, and the variability of the remaining precipitation is greatly reduced compared to the total variability. Additionally, the covariance term is positive in this region. This implies that a large fraction of the rainfall variability along the tropical edge comes from variability in precipitation that comes from tropical lows, suggesting that an
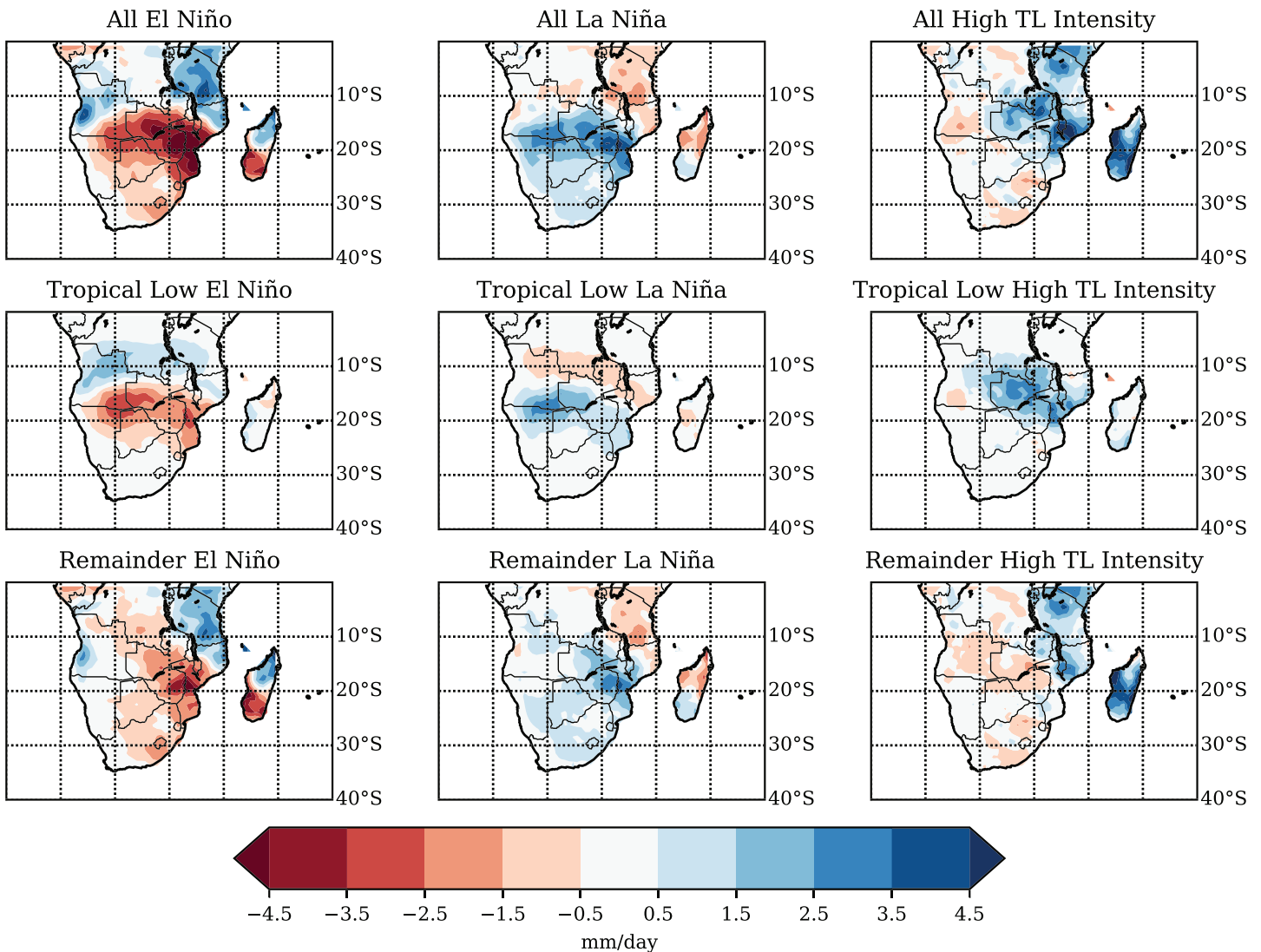
Figure 12. Composite rainfall signal explained by Tropical Lows. Left column: El Niño composite, center column: La Niña composite, right column: High TL Intensity composite. Top row: December, January, and February rainfall anomaly for composite. Middle row: December, January, and February rainfall anomaly of rainfall attributed to tropical lows during composite. Bottom row: December, January, and February rainfall anomaly of rainfall not attributed to tropical lows during composite. Each quantity was calculated independently using tracks from ERA-interim, ERA-5 and MERRA-2, and then averaged over the three reanalysis products. TL = tropical low.

increased understanding of tropical lows may be of value to seasonal forecasting in this region. Notably, this is the region which features more tropical lows during the cool phase of ENSO and less during the warm phase in Figure 7.

In northern Angola and Zambia, although the tropical low rainfall variability is high, the variability of the remainder is not reduced. This is because there is a strong negative covariance between interannual tropical low rainfall and the remaining rainfall. In Figure 7, this is the region where tropical lows are less numerous during La Niña and slightly more numerous during El Niño. Thus, the reduction in the number of tropical lows that occurs in this region during the La Niña phase does not come with a relation in the rainfall in this region because of this negative covariance. This means that in years where there are fewer tropical lows in the northern region, there is more rainfall in the form of mesoscale convective complexes, isolated thunderstorms, and so forth that makes up the difference. In the southern tropical edge, however, in years

without as many tropical lows, or in years where the tropical lows do not rain as much, precipitation from tropical lows is not replaced and the total rainfall is reduced as a result.

Finally, we use the rainfall attribution methodology to examine the composites developed in section 4. For brevity, we present results from CHIRPS only, though similar conclusions were drawn from TAMSAT. Figure 12 shows the anomalous December, January, and February rainfall anomalies for the three composites: El Niño, La Niña, and high TL intensity. Rainfall anomalies are shown in total rainfall, rainfall attributed to tropical lows, and the remaining rainfall that fell more than 5° from a tropical low centroid. The majority of the El Niño and La Niña signals over the interior of southern Africa (west of 30°E) are associated with tropical lows. Further east, the ENSO signal over Mozambique and Tanzania is present in the "remainder" panel. Meanwhile, the high TL intensity composite is associated in increased rainfall over Zambia, Tanzania, and Mozambique. Only the signal over Zambia is attributable to tropical lows.

7. Discussion and Conclusions

Comparisons between three reanalysis products and two gridded rainfall data sets have yielded a set of results which are consistent, through with details that differ. These data sets may be viewed as imperfect reflections of the actual atmosphere. By examining the similarities and differences between the data sets, we are able to assign a qualitative uncertainty estimate to reanalysis features, under the hypothesis that we may be able to ascribe an increased confidence to features that are consistently represented across multiple data sets.

The representation of tropical lows in ERA-5 and MERRA2 is quite similar, with ERA-interim diverging in a number of ways. There are fewer tropical lows that form in ERA-interim than the other two data sets, and their footprint is more spread out. Meanwhile, although there are more separate tropical low events in MERRA-2 than ERA-5, they are typically shorter, possibly because MERRA-2 tropical lows tend to break apart and reform, such that they are double counted with respect to ERA-5. The total number of days with strong tropical lows in MERRA-2 and ERA-5 is remarkably similar (Figure 5). Based on this agreement, and with the knowledge that ERA-5 and MERRA2 are both recent and high-resolution reanalyses, while ERA-Interim is older and of lower resolution, we may decide to trust the representation of tropical lows in MERRA2 and ERA-5 ahead of ERA-Interim.

Common across all data sources, this research has established that tropical lows are important synoptic events which contribute rainfall along the tropical edge of southern Africa. They tend to form from November to March and peak in January. The distribution of track longevity has a long tail, with some tracks lasting up to 30 days, and with a mean duration of 7.5 days. They move eastward and cluster over Angola where they sometimes interact with TTTs, with whom they are not causally linked on a synoptic time scale.

Like the monsoon depressions and tropical lows that have previously been studied in India and northern Australia, southern African tropical lows are an important source of rainfall in the wet season and track predominantly westward. The longevity of southern African tropical lows is longer than in these other regions, however, at 7.5 days as compared to 4–5 days. Similarly, the semistationary nature of the southern African tropical lows appears to be unique, as track density maps in other regions do not show pronounced longitudinal peaks similar to that which occurs over Angola. Howard and Washington (2018) found that tropical lows in Angola interacted with the vorticity stretching of the west coast sea breeze deflected into the middle troposphere by the steep topography, which caused the tropical lows to be anchored in central Angola. We hypothesize that it is this unique anchoring mechanism that causes the difference between southern African tropical lows and those which form in other regions of the tropics. The mean track speed is 4.2 m/s, which is comparable to the speed of Australian lows (6 m/s; Berry et al., 2012), where Australian systems were tracked in isentropic 6-hourly ERA-interim PV. Both eastward and westward moving tropical lows were used to calculate this speed.

Regionally, 31% of November–March rainfall was attributed to tropical lows in summer months along the tropical edge, and the maximum attributable proportion was 66% in south west Angola. This compares well to previous studies based in India and Australia. In India 44% of June–September rainfall has been attributed to low-pressure areas (Hunt & Fletcher, 2019), with a maximum attributable proportion of 60–70% near the north west coast of India. In northern Australia, between 50% and 60% of annual rainfall in the Pilbara has been attributed to closed low-pressure systems (Lavender & Abbs, 2013). Taken together, these results imply

that in the regions where they form frequently over land, tropical lows form a vital component of the local rainfall climatology.

Generally, tropical lows are more numerous in the cool phase of ENSO than the warm phase, although there is a mode of variability that disrupts this relationship, possibly linked to the TEJ. Together with the reduction in tropical low frequency comes a northward shift in tropical low density and rainfall during El Niño and a southward shift during La Niña. This result traces the well known regional ENSO signal to a class of synoptic rain-bearing systems, with the majority of the ENSO rainfall anomaly to the west of 30°E linked to tropical lows (Figure 12). These findings are consistent with studies of the dynamical response of the southern African atmosphere to ENSO. Ratna et al. (2013) characterize this response as a shift in the Walker Circulation over equatorial regions, which leads to enhanced upper level convergence (divergence) over southern Africa during the El Niño (La Niña) phase. This response would lead to a less (more) favorable environment for tropical low formation, since tropical lows feature surface convergence and upper level divergence (Howard & Washington, 2018). Meanwhile, Lindesay et al. (1986) and Vigaud et al. (2009) find that the El Niño phase is associated with a northward shift in the subtropical jet and high-pressure belt, leading to increased subsidence over southern Africa. This subsidence would also inhibit tropical low formation to the south of our region of interest, pushing the locus of tropical lows further north.

This first objective study of tropical lows in southern Africa has identified and tracked cyclonic vortices in Southern Africa and computed the proportion of rainfall that falls within a 5° radius of these systems. It has not speculated on the dynamics of these systems or the mechanisms by which they form. Elsewhere in the tropics, particularly over the tropical ocean basins, equatorial wave theory has been successfully used to attribute tropical rainfall to different modes of wave activity, including Kelvin waves, equatorial Rossby waves, mixed Rossby-Gravity waves, and tropical disturbances (Wheeler & Kiladis, 2002). This paper does not claim that these waves are not important over southern Africa. Indeed, many of these waves, including equatorial Rossby waves and westerly mixed Rossby-Gravity (WMRG) waves, feature vorticity anomalies as key components of their dynamical signals (Kiladis et al., 2009). Therefore, we hypothesize that the tropical lows studied in this paper likely interact with equatorial waves and in some cases may fact be superpositions of various equatorial wave events.

Yang et al. (2018) studied the relationship between AEWs in North Africa and equatorial waves. The equatorial wave methodology rests on the linearization of the dry shallow water equations on a beta plane. The analytic solution to these equations forms a set of basis functions onto which the gridded data sets of observations of the real atmosphere may be projected. Yang et al. (2018) point out that the components of this projection are not necessarily the natural normal modes of an atmospheric structure such as a tropical low or an AEW. They found that, nevertheless, AEWs tend to bear some relation to and are intensified by WMRG waves, although AEWs move more slowly than the WMRGs. A similar study over southern Africa linking equatorial waves (of any flavor) with tropical low would be a key contribution to the field, however, that is beyond the scope of this largely descriptive initial survey.

Further research to determine the processes that drive tropical lows and their relationship with ENSO would improve seasonal forecasts of rainfall in this highly variable region. More clarity on the moisture sources, thermodynamics and vertical structure of these tropical lows would provide insight on their formation and maintenance mechanisms. Diagnosing the representation of tropical lows in climate models will assist in judging the ability of these models to simulate the climate of southern Africa. In particular, the relationship between tropical lows and El Niño offers the prospect of diagnosing problems in climate models that fail to deliver the correct ENSO response in southern Africa (Dieppois et al., 2015). The future change of these systems under anthropogenic climate change must be investigated in order to prepare the tropical edge to adapt to a warmer climate, following the example of Rastogi et al. (2018). This may be achieved by investigating whether they are well represented in CMIP historical simulations and if they are, whether they exhibit coherent change in the corresponding future scenarios.

Appendix A: Sensitivity Analysis

The results of this paper are sensitive to the vorticity threshold criterion applied in Step 3 of the track selection algorithm described in section 2. This criterion was that the filtered vertical mean relative vorticity must

Table A1
Sensitivity Analysis

Parameter	Lower threshold ERA-Interim	Lower threshold ERA-5	Lower threshold MERRA2	Higher threshold ERA-Interim	Higher threshold ERA-5	Higher threshold MERRA2
Threshold (10^{-5} s^{-1})	2.5	2.5	2.5	3.5	3.5	3.5
Reanalysis	ERA-Interim	ERA-5	MERRA2	ERA-I	ERA-5	MERRA2
Track Statistics						
Number per year	50%	38%	40%	−33%	−30%	−29%
Intensity	−8%	−7%	−8%	9%	8%	8%
Longevity	−11%	−9%	−10%	12%	10%	11%
Easterly Track Speed	15%	9%	10%	−14%	−9%	−8%
Interannual						
Number of threshold days per year	53%	42%	38%	−32%	−28%	−27%
Anticorrelation with ENSO	−3%	−27%	−16%	−3%	6%	−3%
Rainfall						
Chirps Average Proportion	11%	7%	9%	−12%	−9%	−8%
Chirps Maximum Proportion	6%	3%	5%	−9%	−6%	−4%
TAMSAT Average Proportion	10%	8%	9%	−12%	−9%	−10%
TAMSAT Maximum Proportion	8%	3%	5%	−10%	−6%	−5%

*Note.*The first three columns show how statistics described by the row name change in each reanalysis when the vorticity threshold is weakened, as compared to the original threshold. The second three columns show the same for when the threshold is strengthened. ENSO = El Niño–Southern Oscillation.

satisfy $\zeta < -3e^{-5}$ s^{-1} in at least one 6-hourly time step. To test the sensitivity to this threshold, all analysis was rerun with threshold values of $2.5e^{-5}$ s^{-1} and $3.5e^{-5}$ s^{-1}.

When the vorticity criterion was weakened, 38–50% more tropical low events are identified, and when it was strengthened, about 30% fewer tracks were present. However, this increase impacted the distribution of TTTs uniformly across space and time. Therefore, all spatial features in the figures remained qualitatively similar as the threshold was varied. The change in key aggregated statistics of all tropical lows is given in Table A1. When a weaker threshold is used, we see more shorter duration, less intense and faster tracks, and a greater proportion of rainfall attributed to tropical lows. The opposite occurs when the threshold is increased. The relationships with ENSO and the TEJ remain significant at a $p < 0.05$ level, although the correlation between ENSO and tropical lows drops in ERA-5 and MERRA-2 when weaker tropical lows are included in the data set. It is worth noting that the proportion of rainfall attributable to tropical lows is much less sensitive to the threshold than the total number of tropical lows identified is.

References

(C3S), C. C. C. S. (2017). ERA5: Fifth generation of ECMWF atmospheric reanalyses of the global climate. Retrieved from https://cds.climate.copernicus.eu

Berry, G. J., Reeder, M. J., & Jakob, C. (2012). Coherent synoptic disturbances in the Australian monsoon. *Journal of Climate*, *25*(24), 8409–8421. https://doi.org/10.1175/JCLI-D-12-00143.1

Blamey, R. C., Kolusu, S. R., Mahlalela, P., Todd, M. C., & Reason, C. J. C. (2018). The role of regional circulation features in regulating El Niño climate impacts over southern Africa: A comparison of the 2015/2016 drought with previous events. *International Journal of Climatology*, *38*(11), 4276–4295. https://doi.org/10.1002/joc.5668

Burpee, R. W. (1974). Characteristics of north African easterly waves during the summers of 1968 and 1969. https://doi.org/10.1175/1520-0469(1974)031<1556:CONAEW>2.0.CO;2

Crétat, J., Pohl, B., Dieppois, B., Berthou, S., & Pergaud, J. (2018). The Angola Low: Relationship with southern African rainfall and ENSO The Angola Low: Relationship with southern African rainfall and ENSO. *Climate Dynamics*, *52*, 1783–1803. https://doi.org/10.1007/s00382-018-4222-3

Dare, R. A., Davidson, N. E., & McBride, J. L. (2012). Tropical cyclone contribution to rainfall over Australia. *Monthly Weather Review*, *140*(11), 3606–3619. https://doi.org/10.1175/MWR-D-11-00340.1

Dee, D. P., Uppala, S. M., Simmons, a. J., Berrisford, P., Poli, P., Kobayashi, S., et al. (2011). The ERA-Interim reanalysis: Configuration and performance of the data assimilation system. *Quarterly Journal of the Royal Meteorological Society*, *137*(656), 553–597. https://doi.org/10.1002/qj.828

Dieppois, B., Rouault, M., & New, M. (2015). The impact of ENSO on Southern African rainfall in CMIP5 ocean atmosphere coupled climate models. *Climate Dynamics*, *45*(9-10), 2425–2442. https://doi.org/10.1007/s00382-015-2480-x

Fine, C. M., Johnson, R. H., Ciesielski, P. E., & Taft, R. K. (2016). The role of topographically induced vortices in tropical cyclone formation over the Indian Ocean. *Monthly Weather Review*, *144*(12), 4827–4847. https://doi.org/10.1175/mwr-d-16-0102.1

Funk, C., Peterson, P., Landsfeld, M., Pedreros, D., Verdin, J., Shukla, S., et al. (2015). The climate hazards infrared precipitation with stations—A new environmental record for monitoring extremes. Retrieved from www.nature.com/scientificdata https://doi.org/10.1038/sdata.2015.66 .

Gelaro, R., McCarty, W., Suárez, M. J., Todling, R., Molod, A., Takacs, L., et al. (2017). The modern-era retrospective analysis for research and applications, version 2 (MERRA-2). *Journal of Climate*, *30*(14), 5419–5454. https://doi.org/10.1175/JCLI-D-16-0758.1

Godbole, RV (1977). The composite structure of the monsoon depression. *Tellus*, *29*(1), 25–40. https://doi.org/10.3402/tellusa.v29i1.11327

Gomes, H. B., Ambrizzi, T., Pontes da Silva, B. F., Hodges, K. I., Silva Dias, P. L., Herdies, D. L., et al. (2019). Climatology of easterly wave disturbances over the tropical South Atlantic. *Climate Dynamics*, *3*, 1393–1411. https://doi.org/10.1007/s00382-019-04667-7

Harrison, M. S. J. (1984). A generalized classification of South African summer rain-bearing synoptic systems. *Journal of Climatology*, *4*(5), 547–560. https://doi.org/10.1002/joc.3370040510

Hart, N. C. G., Reason, C. J. C., & Fauchereau, N. (2010). Tropical-extratropical interactions over southern Africa: Three cases of heavy summer season rainfall. *Monthly Weather Review*, *138*(7), 2608–2623. https://doi.org/10.1175/2010MWR3070.1

Hart, N. C. G., Reason, C. J. C., & Fauchereau, N. (2012). Building a tropical-extratropical cloud band Metbot. *Monthly Weather Review*, *140*(12), 4005–4016. https://doi.org/10.1175/MWR-D-12-00127.1

Hodges, K. I. (1994). A general method for tracking analysis and its application to meteorological data. *Monthly Weather Review*, *122*, 2573.

Hodges, K. I. (1999). Adaptive constraints for feature tracking. *Monthly Weather Review*, *127*, 1362–1373. https://doi.org/10.4324/9781315658032

Hodges, K. I., Cobb, A., & Vidale, P. L. (2017). How well are tropical cyclones represented in reanalysis datasets? *Journal of Climate*, *30*(14), 5243–5264. https://doi.org/10.1175/JCLI-D-16-0557.1

Hopsch, S. B., Thorncroft, C. D., Hodges, K. I., & Aiyyer, A. (2007). West African storm tracks and their relationship to Atlantic tropical cyclones. *Journal of Climate*, *20*(11), 2468–2483. https://doi.org/10.1175/JCLI4139.1

Howard, E., & Washington, R. (2018). Characterizing the synoptic expression of the Angola Low. *Journal of Climate*, *31*(9), 7147–7166. https://doi.org/10.1175/JCLI-D-18-0017.1

Hsieh, J.-S., & Cook, K. H. (2005). Generation of African easterly wave disturbances: Relationship to the African easterly jet. *Monthly Weather Review*, *133*(5), 1311–1327. https://doi.org/10.1175/MWR2916.1

Hunt, K. M. R., & Fletcher, J. K. (2019). The relationship between Indian monsoon rainfall and low-pressure systems. *Climate Dynamics*, *53*, 1859–1871.

Hunt, K. M. R., Turner, A. G., Inness, P. M., Parker, D. E., & Levine, R. C. (2016). On the structure and dynamics of Indian monsoon depressions. *Monthly Weather Review*, *144*(9), 3391–3416. https://doi.org/10.1175/MWR-D-15-0138.1

Hunt, K. M. R., Turner, A. G., & Parker, D. E. (2016). The spatiotemporal structure of precipitation in Indian monsoon depressions. *Quarterly Journal of the Royal Meteorological Society*, *142*, 3195–3210. https://doi.org/10.1002/qj.2901

Hurley, J. V., & Boos, W. R. (2015). A global climatology of monsoon low-pressure systems. *Quarterly Journal of the Royal Meteorological Society*, *141*(689), 1049–1064. https://doi.org/10.1002/qj.2447

Khouakhi, A., Villarini, G., & Vecchi, G. A. (2017). Contribution of tropical cyclones to rainfall at the global scale. *Journal of Climate*, *30*(1), 359–372. https://doi.org/10.1175/JCLI-D-16-0298.1

Kiladis, G. N., Wheeler, M. C., Haertel, P. T., Straub, K. H., & Roundy, P. E. (2009). Convectively coupled equatorial waves. *Reviews of Geophysics*, *47*, 2003. https://doi.org/10.1029/2008RG000266

Kilroy, G., Smith, R. K., & Montgomery, M. T. (2017). Tropical low formation and intensification over land as seen in ECMWF analyses. *Quarterly Journal of the Royal Meteorological Society*, *143*, 772–784. https://doi.org/10.1002/qj.2963

Lavender, S. L., & Abbs, D. J. (2013). Trends in Australian rainfall: Contribution of tropical cyclones and closed lows. *Climate Dynamics*, *40*(1-2), 317–326. https://doi.org/10.1007/s00382-012-1566-y

Levinson, D. H., Knapp, K. R., Kruk, M. C., Howard, J. H., & Kossin, J. P. (2010). The International Best Track Archive for Climate Stewardship (IBTrACS) project: Overview of methods and Indian ocean statistics, *Indian ocean tropical cyclones and climate change* (pp. 215–221). USA: Springer. https://doi.org/10.1175/2009BAMS2755.1

Lindesay, J. A. (1988). South African rainfall, the Southern Oscillation and a Southern Hemisphere semi-annual cycle. *Journal of Climatology*, *8*, 17–30. https://doi.org/10.1002/joc.3370080103

Lindesay, J. A., Harrison, M. S., & Haffner, M. P. (1986). The southern oscillation and South African rainfall. *South African Journal of Science*, *82*(4), 196–198.

Macron, C., Pohl, B., Richard, Y., & Bessafi, M. (2014). How do tropical temperate troughs form and develop over Southern Africa? *Journal of Climate*, *27*(4), 1633–1647. https://doi.org/10.1175/JCLI-D-13-00175.1

Maidment, R. I., Grimes, D., Black, E. C., Tarnavsky, E., Young, M., Greatrex, H., et al. (2017). Erratum: A new, long-term daily satellite-based rainfall dataset for operational monitoring in Africa. Retrieved from www.nature.com/scientificdata https://doi.org/10.1038/sdata.2017.82

McBride, J. L., & Keenan, T. D. (1982). Climatology of tropical cyclone genesis in the Australian region. *Journal of Climatology*, *2*(1), 13–33. https://doi.org/10.1002/joc.3370020103

Mudenda, O. S., & Mumba, Z. L. S. (1996). the unusual tropical storm of January 1996: Zambia Meteorological Department.

Munday, C., & Washington, R. (2017). Circulation controls on southern African precipitation in coupled models: The role of the Angola Low. *Journal of Geophysical Research: Atmospheres*, *122*, 1–17. https://doi.org/10.1002/2016JD025736

Neu, U., Akperov, M. G., Bellenbaum, N., Benestad, R., Blender, R., Caballero, R., et al. (2013). Imilast: A community effort to intercompare extratropical cyclone detection and tracking algorithms. *Bulletin of the American Meteorological Society*, *94*(4), 529–547. https://doi.org/10.1175/BAMS-D-11-00154.1

Ramberg, L., Hancock, P., Lindholm, M., Meyer, T., Ringrose, S., Sliva, J., et al. (2006). Species diversity of the Okavango Delta, Botswana. *Aquatic Sciences*, *68*, 310–337. https://doi.org/10.1007/s00027-006-0857-y

Rastogi, D., Ashfaq, M., Leung, L. R., Ghosh, S., Saha, A., Hodges, K. I., & Evans, K. (2018). Characteristics of Bay of Bengal monsoon depressions in the 21st century. *Geophysical Research Letters*, *45*, 6637–6645. https://doi.org/10.1029/2018GL078756

Ratna, S. B., Behera, S. K., Ratnam, J. V., Takahashi, K., & Yamagata, T. (2013). An index for tropical temperate troughs over southern Africa. *Climate Dynamics*, *41*(2), 421–441. https://doi.org/10.1007/s00382-012-1540-8

Reason, C. J. C., Engelbrecht, F. A., Landman, W. A., Lutjeharms, J. R. E., Piketh, S., Rautenbach, C. J. D. W., & Hewitson, B. C. (2006). A review of South African research in atmospheric science and physical oceanography during 2000-2005: Review article. *South African Journal of Science*, *102*(1–2), 35.

Reason, C. J. C., & Jagadheesha, D. (2005). A model investigation of recent ENSO impacts over southern Africa. *Meteorology and Atmospheric Physics*, *89*(1-4), 181–205. https://doi.org/10.1007/s00703-005-0128-9

Reason, C. J. C., & Keibel, A. (2004). Tropical cyclone Eline and its unusual penetration and impacts over the Southern African mainland. *Weather and Forecasting*, *19*(5), 789–805. https://doi.org/10.1175/1520-0434(2004)019<0789:TCEAIU>2.0.CO;2

Sardeshmukh, P. D., & Hoskins, B. J. (1984). Spatial smoothing on the sphere. *Monthly Weather Review*, *112*, 2524. https://doi.org/10.1175/1520-0493(1984)112<2524:SSOTS>2.0.CO;2

Smith, R. K., & Montgomery, M. T. (2015). Toward clarity on understanding tropical cyclone Intensification. *Journal of the Atmospheric Sciences*, *72*(8), 3020–3031. https://doi.org/10.1175/JAS-D-15-0017.1

Taljaard, J. J. (1953). The mean circulation in the lower troposphere over Southern Africa. *South African Geographical Journal*, *35*(1), 33–45. https://doi.org/10.1080/03736245.1953.10559299

Taljaard, J. J. (1972). Synoptic meteorology of the Southern Hemisphere. In Newton, ChesterW. (Ed.), *Meteorology of the Southern Hemisphere* pp. 139–213). Boston: American Meteorological Society.

Thorncroft, C. D., & Hoskins, B. J. (1995). An idealized study of African easterly waves. II: A nonlinear view. *Quarterly Journal of the Royal Meteorological Society*, *121*(527), 1589–1614. https://doi.org/10.1002/qj.49712152706

Todd, M. C., & Washington, R. (1999). Circulation anomalies associated with tropical-temperate troughs in southern Africa and the south west Indian Ocean. *Climate Dynamics*, *15*(12), 937–951. https://doi.org/10.1007/s003820050323

Vigaud, N., Richard, Y., Rouault, M., & Fauchereau, N. (2009). Moisture transport between the South Atlantic Ocean and southern Africa: Relationships with summer rainfall and associated dynamics. *Climate Dynamics*, *32*(1), 113–123. https://doi.org/10.1007/s00382-008-0377-7

Wallace, J. M. (1971). Spectral studies of tropospheric wave disturbances in the tropical western Pacific. *Reviews of Geophysics*, *9*(3), 557–612. https://doi.org/10.1029/RG009i003p00557

Wheeler, M., & Kiladis, G. N. (2002). Convectively coupled equatorial waves: Analysis of clouds and temperature in the wavenumber frequency domain. *Journal of the Atmospheric Sciences*, *56*(3), 374–399. https://doi.org/10.1175/1520-0469(1999)056<0374:ccewao>2.0.co;2

Wilks, D. (2016). The stippling shows statistically significant grid points: How research results are routinely overstated and overinterpreted, and what to do about it. *Bulletin of the American Meteorological Society*, *97*(12), 2263–2273. https://doi.org/10.1175/BAMS-D-15-00267.1

World Bank (2010). The Zambezi river basin. A multi-sector investment opportunities analysis. Volume 3. State of the Basin. Africa.

Yang, G.-Y., Methven, J., Woolnough, S., Hodges, K. I., & Hoskins, B. J. (2018). Linking African easterly wave activity with equatorial waves and the influence of Rossby waves from the Southern Hemisphere. *Journal of the Atmospheric Sciences*, *75*, 1783–1809. https://doi.org/10.1175/jas-d-17-0184.1